2020-01-20

Concentration Dependent Diffusion of Solvent in Heavy Oil

Carril Naranjo, José Eduardo

UNIVERSITY OF CALGARY

Concentration Dependent Diffusion of Solvent in Heavy Oil

by

José Eduardo Carril Naranjo

A THESIS

SUBMITTED TO THE FACULTY OF GRADUATE STUDIES

IN PARTIAL FULFILMENT OF THE REQUIREMENTS FOR THE

DEGREE OF MASTER OF SCIENCE

GRADUATE PROGRAM IN CHEMICAL AND PETROLEUM ENGINEERING

CALGARY, ALBERTA

JANUARY, 2020

ABSTRACT

In recent years, solvent-based methods have arisen as a feasible alternative to thermal schemes for heavy oil recovery, owed to the diffusive solvent mass transfer effect on oil mobility. The increasing incorporation of significant diffusion physics to models describing the process will lead to successful field implementations.

In this work, a numerical model that captures the solvent diffusion coefficient dependence, on its concentration in solvent – bitumen / heavy oil systems, was developed and tested.

The *interFoam* solver was enabled to account for two phases and a miscible component diffusing between them. Then, one-dimensional diffusion simulations were conducted to validate its results against analytical solutions.

Once the two phases and miscible component diffusion features were validated, the solvent diffusivity concentration dependence feature was added to the numerical model. This attribute was later evaluated against experimental measurements of solvent concentration evolution in heavy oil and bitumen. To this end, results from two experimental works were considered as reference.

This study demonstrates that the diffusivities observed in the solvent – heavy oil / bitumen systems analysed can be numerically handled by the model presented. Additionally, the solvent concentration dependence feature makes of the model an important tool to evaluate its effect on viscous oil and it can potentially be implemented in pore scale models.

ACKNOWLEDGEMENTS

I want to express my sincere gratitude to my supervisor Dr. Apostolos Kantzas without whose support it would not have been possible to complete this project. He was always willing to listen and guide me patiently in every situation along this process.

I have no words to thank Carla Sena for all the time she spent guiding me, giving me advice and even giving me words of encouragement during the preparation of this work.

Additionally, I want to thank Dr. Roberto Aguilera and Dr. Brij Maini for being part of my committee, for taking time to read my thesis. Their comments and suggestions greatly enriched my work.

I would like to thank my mother for her love and constant support regardless of the circumstances, my father and my brothers for their support and subtle way of pressing, and the rest of my family for always being there.

Special acknowledgements to PEMEX and the Mexican National Council for Science and Technology (CONACyT) for their financial support.

Finally, I want to thank the University of Calgary and Fundamentals of Unconventional Resources Group (FUR), colleagues and friends for their advice, comments and particularly the day-to-day coexistence, which made of this an enjoyable experience.

TABLE OF CONTENTS

ABSTRACT ii

TABLE OF CONTENTS iv

LIST OF TABLES vi

LIST OF FIGURES vii

NOMENCLATURE ix

Chapter 1. Introduction 1

1.1. Background 1

1.2. Objectives 7

1.3. Layout 8

Chapter 2. Methodology 10

2.1. Numerical Scheme 10

2.2. OpenFoam 13

2.3. Governing equations 14

2.4. Interfacial diffusion approach 19

2.5. Diffusion coefficient 23

Chapter 3. Model Validation 24

3.1. Grid refinement effect. 25

3.2. Diffusivity range 28

3.3. Interfacial mass transfer 31

Chapter 4. Concentration dependent mass transfer simulations. 40

4.1. Slopes and intercepts model 40

4.2. Vignes modified model 41

4.3. Experiments description and modeling. 46

4.3.1. Salama's experiments. 46
4.3.2. Computational domain. 47
4.3.3. Diedros's experiments. 48
4.3.4. Computational domain 49
4.4. Concentration profiles evolution 50
4.5. Experiment vs. Modeling 52
4.5.1. Salama's experiment modeling 52
4.5.2. Diedro's experiment modeling 60
CHAPTER 5. CONCLUSIONS AND FUTURE WORK 65
5.1. FINAL CONCLUSIONS 65
5.2. RECOMMENDATIONS 66
References 67

LIST OF TABLES

Table 3.1 Diffusivity range evaluation 28

Table 3.2 Diffusivity range evaluation 31

Table 3.3 Convective and diffusive fluxes effect. 38

Table 4.1 Vignes Modified model ‘acceleration’ and ‘deceleration’ parameters. 43

Table 4.2 Hexane system concentration profile data. 45

Table 4.3 Fluids viscosities for Salama's experiment. 46

Table 4.4 Fluids viscosities for Diedro's experiments 49

LIST OF FIGURES

Figure 1.1 Modeling methods for interface description (Versteeg and Malalasekera 2007) 10

Figure 2.1 Fluids parameters and volume fraction distribution in a 2D computational domain. 17

Figure 3.1 One-dimension diffusion. 24

Figure 3.2 Grid refinement effect $\mathrm{D} = 1\mathrm{E} - 9\mathrm{m2s}, \mathrm{t} = 5\mathrm{s}.$ 26

Figure 3.3 Grid cells test $(\mathrm{D} = 1\mathrm{E} - 9\ \mathrm{m2/s}, \mathrm{t} = 5\mathrm{s})$. 27

Figure 3.4 Concentration profiles, $(\mathrm{D} = 1\mathrm{E} - 5\ \mathrm{m2/s})$. 29

Figure 3.5 Concentration profiles, $(\mathrm{D} = 1\mathrm{E} - 7\ \mathrm{m2/s})$. 29

Figure 3.6 Concentration profiles, $(\mathrm{D} = 1\mathrm{E} - 9\ \mathrm{m2/s})$. 30

Figure 3.7 Concentration profile, $(\mathrm{D} = 1\mathrm{E} - 11\ \mathrm{m2/s})$ 30

Figure 3.8 Infinite composite medium. 32

Figure 3.9 Two phases numerical description. a) Indicator phase function, b) Average volume of the magnitude in the cell (Haroun 2008). 33

Figure 3.10 Interphase digital representation. 34

Figure 3.11 $\mathrm{D1} = \mathrm{D2} = 1\mathrm{E} - 5\ \mathrm{m2/s}, \mathrm{t} = 0.002\ \mathrm{s}.$ 35

Figure 3.12 $\mathrm{D1} = \mathrm{D2} = 1\mathrm{E} - 7\ \mathrm{m2/s},\ \mathrm{t} = 0.2\ \mathrm{s}.$ 36

Figure 3.13 $\mathrm{D1} = \mathrm{D2} = 1\mathrm{E} - 9\ \mathrm{m2/s},\ \mathrm{t} = 20\ \mathrm{s}$ 36

Figure 3.14 $\mathrm{D1} = \mathrm{D2} = 1\mathrm{E} - 11\ \mathrm{m2/s},\ \mathrm{t} = 2000\ \mathrm{s}.$ 37

Figure 3.15 concentration profiles $(\mathrm{D1} = 1\mathrm{E} - 7, \mathrm{D2} = 1\mathrm{E} - 6\ \mathrm{m2/s})$ 39

Figure 4.1 Diffusion coefficient for n-hexane, n-heptane and n-octane in heavy oil at 25℃, Slopes and Intercepts (Guerrero-Aconcha 2009). 41

Figure 4.2 Diffusion coefficient for n-hexane, n-heptane and n-octane in heavy oil at 25℃, Vignes Modified. 43

Figure 4.3 Region of interest and initial fluids distribution (Salama 2006). 47

Figure 4.4 Salama's experiment computational domain. 48

Figure 4.5 Holder dimensions and fluids distribution. 49

Figure 4.6 Computational domain for Diedro's experiment. 50

Figure 4.7 Mixing zone length with time (octane-oil), (Salama 2006). 51

Figure 4.8 Concentration profiles for hexane in heavy oil (1:05 h). 53

Figure 4.9 Concentration profiles for hexane in heavy oil (7:10 h). 53

Figure 4.10 Concentration profiles for hexane in heavy oil (28:15 h). 54

Figure 4.11 Concentration profiles for heptane in heavy oil (1:05 h). 54

Figure 4.12 Concentration profiles for heptane in heavy oil (7:10 h). 55

Figure 4.13 Concentration profiles for heptane in heavy oil (28:15 h). 55

Figure 4.14 Concentration profiles for octane in heavy oil (1:05 h). 56

Figure 4.15 Concentration profiles for octane in heavy oil (7:10 h). 56

Figure 4.16 Concentration profiles for octane in heavy oil (28:15 h). 57

Figure 4.17 Absolute errors between simulated and measured concentration data, Salama's experiment. 58

Figure 4.18 Increase of the length of the mixing zone (Salama 2006). 59

Figure 4.19 Concentration profiles for Peace River bitumen and DME (0.1 day). 62

Figure 4.20 Concentration profiles for Peace River bitumen and DME (1 day). 62

Figure 4.21 Concentration profiles for Grosmont bitumen and DME (0.1 day). 63

Figure 4.22 Concentration profiles for Grosmont bitumen and DME (1 day). 63

Figure 4.23 Absolute errors between simulated and measured concentration data. 64

NOMENCLATURE

C	Species concentration, fraction
C_1	Species concentration in fluid 1, fraction
C_2	Species concentration in fluid 2, fraction
C_o	Initial species concentration, fraction
C_s	Solvent concentration, fraction
c_i	Mass fraction of component i or solvent, fraction
c_j	Mass fraction of component j or bitumen, fraction
D	Diffusion coefficient, m^2/s
D_1	Diffusion coefficient fluid 1, m^2/s
D_2	Diffusion coefficient fluid 2, m^2/s
D_{ij}	Mutual diffusion coefficient of components i and j, m^2/s
D_{ij}^{∞}	Diffusion coefficient at infinite dilution of component j in i, m^2/s
D_{ji}^{∞}	Diffusion coefficient at infinite dilution of component in i in j, m^2/s
He	Henry's law constant, dimensionless
X_A	Analytical value
X_N	Numerical value

C-LS	Color-Level Set
CDDP	Concentration Dependent Diffusion Coefficient
CF-VOF	Color Function-Volume of Fluid Method
CFD	Computational Fluid Dynamics

CHOPS	Cold Heavy Oil Production with Sands
CSF	Continuum Surface Force
CSI	Cyclic Solvent Injection
CT	Computed Tomography
DME	Di Methyl Ether
IR-VOF	Interface Reconstruction – Volume of Fluid Method
REV	Representative Elementary Volume
ROI	Region of Interest
SIMPLE	Semi-Implicit Method for Pressure-Linked Equations
VAPEX	Vapour Extraction
VM	Vignes Modified
VOF	Volume of Fluid Method

β	Acceleration parameter of solvent in diffusion coefficient
δ	Deceleration parameter of bitumen in diffusion coefficient
ε_a	Absolute error, dimensionless
ε_a	Absolute error, dimensionless
ρ_B	Bitumen density, kg/m^3
ρ_{mix}	Mixture density, kg/m^3
ρ_S	Solvent density, kg/m^3

CHAPTER 1. INTRODUCTION

1.1. BACKGROUND

After primary and secondary production stages, heavy oil and bitumen recovery essentially depends on mechanisms that decrease their in-situ viscosity (Guo, Li, and Yu 2016). To this end, thermal techniques have prevailed due to the strong relation between temperature and viscosity, where the steam based processes is preferred due to their capability to readily deliver important amounts of heat (Wang et al. 2018). However, in some heavy oil reservoirs, the water content, reservoir properties heterogeneity and formation thickness, may constraint their effectiveness (Butler and Mokrys 1991; Du, Peng, and Zeng 2018). Moreover, the high water and energy requirements, water post process treatment cost, and CO_2 emissions (Du et al. 2018), are against the energy conservation and emissions reduction global penchant. (Guo et al. 2016).

These reasons have encouraged researchers to find a way to overcome the shortcomings of thermal processes. In this context, viscosity reduction through solvent dissolution (Luo, Yang, and Gu 2007) has arisen as a worthwhile alternative, due to the analogy existent between mass transfer by diffusion and heat transfer by conduction (Butler and Mokrys 1989).

In the last 60 years, a variety of schemes using solvent to recover heavy oil and bitumen have been proposed (Bayestehparvin, Farouq Ali, and Abedi 2018). Solvent injection into the

reservoir is intended at improving the steam-based processes, reduce steam supply or completely replace it by solvent. Based on the fluids configuration employed, these can be classified as solvent-aided or solvent-based procedures (Ardali, Barrufet, and Mamora 2012; Bayestehparvin et al. 2018).

Solvent injection not only avoids the high pressures and temperatures needed by steam based methods (Butler and Mokrys 1989). In addition, it may even beat some other methods performance when applied to thin reservoirs, where heat losses to base and caprock make the required steam/oil ratio prohibitively high; reservoirs underlying aquifers, where thermal energy may be released to the aquifer rather than the oil; or offshore fields, due to operational hazards and area requirements for steam generation (Das 1998).

Experimental, numerical and field tests have demonstrated that processes using solvents can improve the viscous oil recovery. However, for those using only solvent (i.e. Vapour Extraction, VAPEX), the pressures needed to increase its solubility, in addition to the limited gravity drainage existing in thin reservoirs, promote low production rates, which compromise their economic viability (Das 1998; Jamaloei et al. 2013; Pourabdollah and Mokhtari 2013; Qi and Polikar 2005).

Alternatives to speed up the solvent effect and to increase the production rates are the cyclic solvent injection (CSI) processes. These approaches rely on the involvement of several driving mechanisms triggered by the solvent and heavy oil or bitumen interaction. Among them, viscosity reduction, foamy oil flow and solution gas drive, are considered as the most relevant ones (Du et al. 2018; Zhou et al. 2018). The greater recovery rates obtained by the action of these mechanisms, in addition to the possibility to be applied in no thermally

completed wells, make them a potential follow up heavy oil recovery process to Cold Heavy Oil Production with Sand (CHOPS) implementations (Ahadi and Torabi 2018; Chang and Ivory 2013).

Nevertheless, despite the proven plusses of solvent-based methods, drawbacks are not solved yet. They have lower oil recovery rates compared to those of thermal techniques, in addition to the elevated solvent costs, which jeopardize their massive usage (Butler and Mokrys 1991).

Intended to solve these limitations, solvent aided methods have emerged as the option to obtain sufficiently high oil recovery rates with moderate water and energy consumption and lesser solvent expenses. Solvent-aided methods attain the heavy oil and bitumen viscosity reduction through the steam properties, which performance is improved by the addition of hydrocarbon additives (solvent) that, at the same time, diminish the steam consumption (Lin et al. 2014).

An important step in the design of these recovery methods is the solvent selection. A proper screening should consider the following: The application modality intended, reservoir characteristics where it will be applied, heavy oil or bitumen properties, and cost and solvent availability.

Most of these approaches rely on solvents in their gaseous phase (Allen et al. 1976; Bardon, Karaoguz, and Tholance 1986; Butler and Mokrys 1989; Das and Butler 1996; Nasr et al. 2002; Sabeti et al. 2015; Zhao 2004). However, the ability of liquid solvents to completely mix with oil, and their capability to reduce heavy oil and bitumen viscosity with minimal asphaltenes precipitation (mixing quality), are attracting the researcher's attention to use them as recovery agents in oil sands and fractured reservoirs, despite their low diffusion rate

(Haddad, Hejazi, and Gates 2017; Leyva-Gomez and Babadagli 2018; Marciales and Babadagli 2016).

Both, mixing quality and mass transfer diffusion rate, are crucial design parameters for heavy oil or bitumen recovery through liquid solvents. Therefore, a detailed knowledge about their combined effect on the process becomes compulsory. Diffusion rate, for instance, may limit the whole process performance due its low values (Fadaei, Shaw, and Sinton 2013; Guerrero-Aconcha 2009; Keshmiri et al. 2019).

The rate at which the mass is transferred is controlled by the molecular diffusion coefficient, which can be estimated from measurements conducted through direct or indirect methods. Direct methods consist on conducting compositional analysis of heavy-oil or bitumen mixed with solvent at different times and locations during a diffusion test (Diedro et al. 2015). Indirect measurements, on the other hand, measure parameters associated to heavy oil–solvent or bitumen–solvent mixtures, such as: Pressure, interface velocity and position, magnetic field strength and diffusing solute volume, changes that reflect the solvent mass transferred into oil (Guerrero-Aconcha 2009; Sheikha, Pooladi-Darvish, and Mehrotra 2005).

Nevertheless, the difficulty to obtain good quality measurements and the challenge that represents a suitable data interpretation, the lower time and cost of data acquisition, in addition to a higher resolution, have made of the indirect techniques the preferred by researchers (Ghanavati, Hassanzadeh, and Abedi 2014).

In some cases, the diffusion coefficient can be reasonably considered as constant (dilute solutions). However, as fluids become denser and more complex, it varies as a function of solvent concentration in the mixture (Hayduk and Cheng 1971), and viscosity of the fluid

into which it diffuses (Crank 1979; Guerrero-Aconcha 2009).

As mixture viscosity increases due to growing concentration of the more viscous constituent, the mobility of diffusing molecules decreases. Then, it would be expected that the diffusion coefficient decrease as the mixture viscosity increases and vice versa. Taking this into account, a unique diffusion coefficient over a wide concentration range should not be assumed (Ghanavati et al. 2014). Moreover, neglecting the diffusion coefficient solvent concentration dependency, could lead to unrealistic results (Das and Butler 1996; Keshmiri et al. 2019). Interestingly, some methods that consider the dependency on solvent concentration to obtain the diffusion coefficient in heavy oil or bitumen have not resembled this idea (Fadaei et al. 2013; Ghanavati et al. 2014).

For example, the approach proposed by Boltzmann (Boltzmann 1894) and Matano (Matano 1933), have delivered results that differ from the expectative of diffusion coefficient increasing as solvent concentration does (Oballa and Butler 1989; Salama 2006; Wen and Kantzas 2005). In these approaches, an initial rising tendency of the diffusion coefficient was observed, which severely drops as solvent concentration approaches to intermediate values in the range from 0 to 1 of solvent concentration.

In this context, after thoroughly reviewing, a number of research work showing a not consistent increasing or decreasing relation between diffusivity and solvent concentration. Guerrero (Guerrero-Aconcha 2009) suggested that behaviour similar to that of less complex or binary systems should be expected in solvent-heavy oil and solvent-bitumen systems.

In order to confirm his hypothesis and find a way to reproduce this performance, he estimated diffusion coefficients of C6, C7 and C8 in heavy oil. From density profiles (Salama 2006),

diffusivity values were calculated through the “Slopes and Intercepts model” (Sarafianos 1986), which showed the expected increasing tendency as solvent concentration increased (Guerrero-Aconcha 2009).

The confirmation of the existent relationship between diffusion coefficient and solvent concentration modifies the diffusion process understanding of hydrocarbon solvents in highly viscous fluids. Consequently, an extensive evaluation about this characteristic is required before full field implementations.

A critical step in a proper design of any enhanced oil recovery development is to conduct simulations. This refers to the process of infer the performance of a real system from physical or mathematical models which, in order to be representative, should adequately describe the physics taking place in the system (Graveleau 2016; Peaceman 2000).

To build models of real size, whether physical or mathematical, would be impractical. Therefore, these are typically defined in representative elementary volumes (REV) of the system, which are defined of as the minimum volume needed to obtain accurate calculations for an averaged quantity.

Nevertheless, these are meant to provide effective representations of the microscopic physics at scales larger than the pore scale continuum (Cinar and Riaz 2014), variables governing the multiphase flow in porous medium such as gravity, capillary and viscosity ratio effects, in addition to those occurring at pore level interfaces, are not necessarily captured (Graveleau 2016). Therefore, in order to improve them, new approaches should capture detailed physical descriptions of fluids interaction and flow through the microscopic pore space (Cinar and Riaz 2014).

1.2. OBJECTIVES

To build a numerical model in the Computational Fluid Dynamic (CFD) open source code OpenFOAM; based on the multiphase solver *interFoam* which tracks the interface progress between incompressible, miscible and isothermal fluids, using the Volume of Fluid (VOF) approach.

The numerical model should be able to simulate hydrocarbon solvent diffusion in bitumen and heavy oil, considering the diffusion coefficient dependence on solvent concentration.

1.3. LAYOUT

Chapter 1 presents the background and purpose of investigate the solvent concentration effect on the diffusion coefficient and to be captured in a numerical model.

In Chapter 2, the numerical scheme chosen to develop this work and its governing equations are presented, as well as, the multiphase and interfacial diffusion approaches used.

Chapter 3 includes the workflow to validate the numerical model. First, the grid refinement effect was evaluated. Therefore, the model capability to handle diffusivities typically observed in solvent – heavy oil / bitumen systems was assessed. Lastly, the interfacial diffusion feature, enabled for the numerical model, was tested.

In Chapter 4, the models used to estimate the diffusion coefficient accounting for the solvent concentration are presented. Additionally, the setting of the experiments to be simulated and the computational models are described. Finally, results from simulations are compared to those of the experimental measurements.

In Chapter 5, conclusions from this study and main findings are provided. Likewise, recommendations for future work are presented.

In this work, a CFD OpenFOAM model was enabled to conduct simulations of solvent diffusion in heavy oil and bitumen. The *interFoam* solver was enabled to handle interfacial diffusion, and for first time in our research group, Fundamental Unconventional Resources (FUR), and as far as we know in the literature, the diffusion coefficient solvent concentration

dependence, was considered under the OpenFOAM framework. Besides, the results were validated with experimental measurements.

CHAPTER 2. METHODOLOGY

2.1. NUMERICAL SCHEME

In multi-phase systems, processes occurring at micro scale are meaningful on fluids behaviour at larger scale. Aimed to increase the understanding of these phenomena, different modeling approaches have been developed. Either from Eulerian or Lagrangian points of view, their features make them suitable alternatives depending on the application.

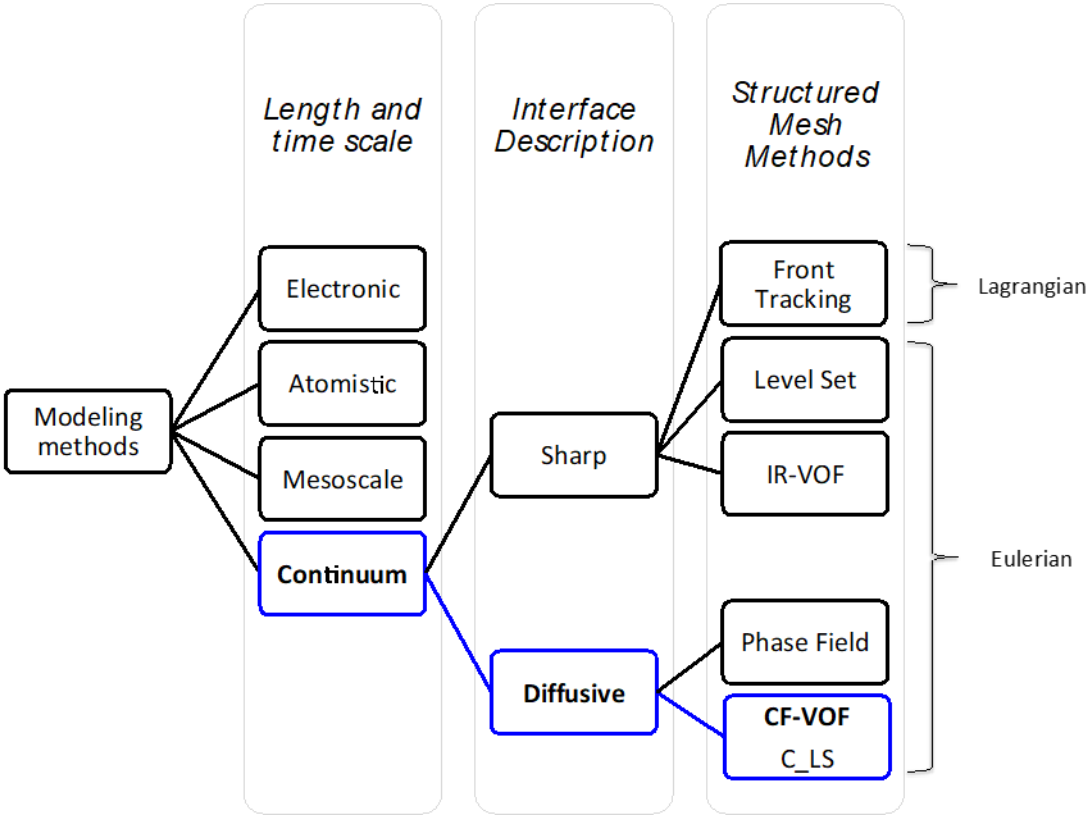

Figure 1.1 Modeling methods for interface description
(Versteeg and Malalasekera 2007)

In Figure 1.1 different modeling approaches are classified based on the scale upon they are defined. The three first groups correspond to different organization levels, where elementary particles, atoms and molecules are regarded as matter, which behaviour is described by quantum mechanics and statistical mechanics laws.

In the last group, the assumption of the fluid as a continuum is based on the length scale of the system analysed, so that, if the associated dimensionless Knudsen number (Kn) remains smaller than one, molecules structure and motion do not influence their macroscopic properties (velocity, pressure, density and temperature). Furthermore, a suitable control volume scale allows enclosing a large enough number of molecules, which averaged properties well represent the fluid behaviour through the continuity and momentum conservation equations (Versteeg and Malalasekera 2007).

Depending on how the interfaces are represented in a computational domain, continuum methods are organized in two groups, sharp and diffuse. In sharp interface methods, a zero-thickness interface implies a discontinuity in the properties of the fluids. Diffuse interface methods, on the other hand, describe the interface into a region of finite thickness where fluid properties change gradually.

Sharp and diffusive interface methods rely on a structured grid to solve the momentum equation, which implicitly dictates interface motion across the computational domain, either applied from Eulerian or Lagrangian approaches. In Lagrangian methods, the individual movement of particles that together define the interface, describe its general movement. Eulerian methods, instead, describe the interface through a scalar function built in the mesh.

Despite their high accuracy and ease to implement boundary conditions at the interfaces,

Lagrangian methods are limited to simple topologies. Therefore, since the complexity observed in processes at pore scale, Eulerian methods are preferred due their compatibility with CFD packages and the variety of interface tracking techniques they support. As the most popular, the following can be mentioned:

Level Set (Osher and Sethian 1988): In this approach the interface motion is defined by a smooth function, $\varphi(x,t)$, positive at one side of it, negative at the other, and equal to zero at the interface. At later times, the interface position is captured by interpolation between grid points. Nevertheless, complex shapes, breaking, and coalescence of interfaces are well handled; level set methods undergo unphysical mass fluid losses as time evolves (Luo et al. 2015).

Phase field: Each phase is characterized by a phase field parameter, φ, which takes φ_- or φ_+ values in bulk phases and changes gradually across transition region. The interface location is defined by $(\varphi_- + \varphi_+)/2$ and its motion is modeled through the Cahn-Hilliard equation.

$$\frac{\partial \varphi}{\partial t} + (u \cdot \nabla)\varphi = \nabla \cdot \left(M \nabla \mu_\varphi\right) \quad (1)$$

Where $M(\varphi)$ is the diffusion parameter (mobility) and μ_φ stands for the chemical potential (Wörner 2012). This approach can capture interfaces coalescence and break up. Besides, mass is conserved along the simulation time. Nonetheless, solution of Cahn Hilliard equation is numerically complex and computational expenses increase when relevant physics are modeled (Badalassi, Ceniceros, and Banerjee 2003)

Volume of fluid (Hirt and Nichols 1981): In this approach the two-phase flow is considered

as a single-phase flow, in which properties vary with an indicator function representing the volume fraction of one phase in the computational domain. Grid cells occupied by phase 1 have a value of $\alpha = 1$, whereas cells occupied by phase 2 take a value of $\alpha = 0$; cells containing the interface have a value of α between 0 and 1. The interface motion is described by simultaneously solving the continuity, momentum and advection equations for volume fraction. This method's popularity is due to only one convective equation must be solved to estimate the volume fraction of each cell as fluids flow. In addition, the volume conservation is guaranteed and therefore so does the mass. Nevertheless, wrong selection of the advection schemes may compromise the interfaces sharpness and solution stability (Emad 2014; Márquez-Damián n.d.).

Since its mass conservative nature and capability to account for sub-pore scale physics such as mass transfer, in addition to its convenience when implemented in open source systems, the VOF method was chosen to be used in this work.

2.2. OpenFOAM

Open source systems have attracted a lot of attention since they allow adapting codes according to user's requirements. OpenFOAM is an open source CFD code that provides libraries and applications for solution of continuum mechanic problems. Among several solvers, it provides the multiphase solver *interFoam*, which tracks the interface progress between incompressible, immiscible and isothermal fluids using the VOF method.

This is numerically solved by using a Finite Volume method, where different discretization

techniques may be used. For transient simulations, pressure-velocity coupling needed to solve the NS equations is handled by the SIMPLE (Semi-Implicit Method for Pressure-Linked Equations) loop. Additional equations not related to the loop are solved after the pressure and velocity fields are calculated. The OpenFOAM cases are structured as directories. In the system *directory*, the numerical schemes, equation solvers and run parameters are set up (Santiago 2015).

The *interFoam* solver, a Volume of Fluid based numerical method, is used in this work to model the diffusion process of a hydrocarbon solvent in bitumen, where the concentration of components in each phase varies due to interfacial mass transfer.

2.3. GOVERNING EQUATIONS

Two-phase flow is defined as the interactive flow of two materials in the same or different state with a common interface, each with its own properties. Under static conditions, these phases will describe a definite interface, which agrees with the physical configuration of the problem to be simulated.

In accordance to the numerical representation proposed, the concentration evolution of a miscible component between these two phases, can be analysed as a single-phase problem.

Two-phase flows are usually modeled through the continuity and momentum Navier Stokes equations, that applied for solvent (s) and bitumen (b) phases, analysed in this work, become:

$$\frac{\partial \rho_i}{\partial \mathrm{t}} + \nabla \cdot (\rho_i v_i) = 0 \qquad i = s, b \qquad (2)$$

$$\frac{\partial (\rho_i v_i)}{\partial t} + \nabla \cdot (\rho v_i v_i) = -\nabla p_i + \rho_i g + \nabla \cdot [\mu_i (\nabla v_i + (\nabla v_i)^T)] \qquad i = s, b \qquad (3)$$

Where ρ, v, p, g and μ are fluid density, fluid velocity, pressure, gravity and fluid viscosity, respectively.

For continuity equation (2), the first term in the left hand side corresponds to the rate of change in mass per unit volume, whereas the second one, is the net flow of mass out of the element across its boundaries (Versteeg and Malalasekera 2007). Since fluids involved are assumed to be incompressible, density and viscosity are assumed as constant, therefore continuity equation becomes:

$$\nabla \cdot v_i = 0 \qquad i = s, b \qquad (4)$$

For which boundary conditions at the interface between fluids and with not reactive solids are respectively:

$$\rho_i (\boldsymbol{v} - v_i) \cdot \boldsymbol{n}_{sb} = 0 \qquad i = s, b \qquad (5)$$

$$\boldsymbol{n}_{Sol} \cdot v_i = 0 \qquad i = s, b \qquad (6)$$

Where $\boldsymbol{v}$ is the interface velocity, $\boldsymbol{n}_{sb} = n_s cos\theta + \boldsymbol{n_t} sin\theta$ is the normal to the interface from solvent phase to bitumen phase and $\boldsymbol{n}_{Sol}$ is the normal to the solid, (Bothe and Warnecke 2005; Graveleau 2016).

Momentum equation, on the other hand, incorporates the momentum added by advection per unit volume in the second term, and its rate of change in the first one, for the left-hand side of the equation. Pressure, gravitational and viscous forces are depicted in the right hand side of it (Versteeg and Malalasekera 2007)

In this case, the boundary conditions at the interface are:

$$\begin{aligned} \boldsymbol{n}_{sb}[-\rho_s(v_s-\boldsymbol{v})v_s - Ip_s + \mu_s(\nabla v_s + (\nabla v_s)^T)] \\ = \boldsymbol{n}_{sb}[-\rho_b(v_b-\boldsymbol{v})v_b - Ip_b \\ + \mu_b(\nabla v_b + (\nabla v_b)^T)] + H_{sb}\sigma\boldsymbol{n}_{sb} \end{aligned} \tag{7}$$

Where I stands for unity tensor, H_{sb} interface curvature and σ is the surface tension.

The boundary conditions at solid surface for two-phase flows are for each phase:

$$v_i = 0 \qquad i = s, b \tag{8}$$

These equations are solved through the finite volume approach, which rely in the Volume of Fluid method to capture the interface dynamics. This technique depicts the phase's distribution through an indicator function, α, that represents the volume of the phases present in each cell (Luo et al. 2015; Osher and Sethian 1988; Wörner 2012).

According to this distribution the fluid density and viscosity can be defined as:

$$\rho(\alpha) = \alpha\rho_b + (1-\alpha)\rho_s \tag{9}$$

$$\mu(\alpha) = \alpha\mu_b + (1-\alpha)\mu_s \tag{10}$$

Figure 2.1 shows the values that α can take depending on the phase's occupancy.

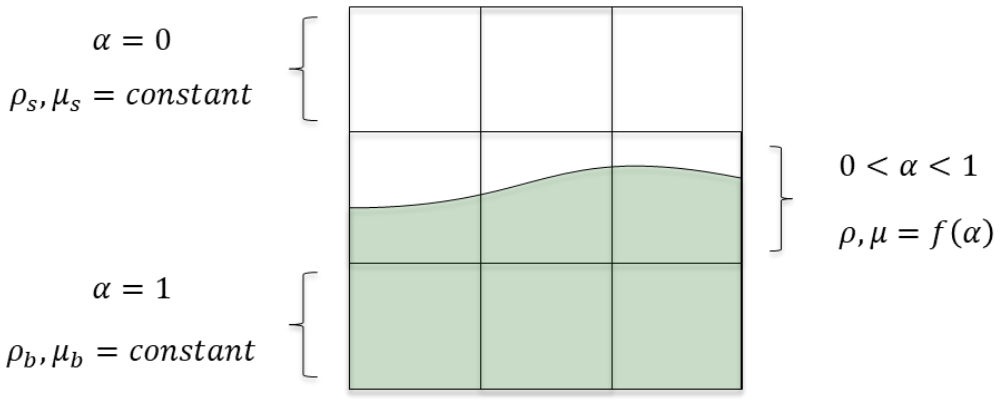

Figure 2.1 Fluids parameters and volume fraction distribution in a 2D computational domain.

The indicator function definition (9), can be used to describe the density field in the continuity equation (2), so that:

$$(\rho_s - \rho_b)\frac{\partial \alpha}{\partial \mathrm{t}} + \nabla \cdot \big((\rho_s - \rho_b)\alpha v\big) + \rho_b v = 0 \qquad i = s, b \qquad (11)$$

This derives in the "Advection of the volume fraction field" governing equation that describes the evolution of the interface (Deshpande, Anumolu, and Trujillo 2012; Groß and Reusken 2013; Santiago 2015).

$$\frac{\partial \alpha}{\partial \mathrm{t}} + \nabla \cdot (\alpha v) = 0 \qquad (12)$$

The discontinuity of fluids properties (ρ,μ) across the interface, leads to interface spreading and increases the computational cost when this is numerically solved. Aimed to mitigate this trouble, an artificial compression term is added to equation (12) which influence degree can be controlled through an input constant in *interFoam*.

$$\frac{\partial \alpha}{\partial \mathrm{t}} + \nabla \cdot (\alpha v) + \nabla \cdot (\alpha(1-\alpha)v_r) = 0 \tag{13}$$

Where v_r, is the artificial compression velocity.

A convenient method for numerical simulations of incompressible two-phase flows is the one fluid model. In this method, an interface representation, as the mentioned above, and a single momentum equation valid in the whole domain are required. Composed of variables defined at the center of each cell, the momentum reads (Graveleau 2016; Groß and Reusken 2013; Santiago 2015):

$$\rho\left(\frac{\partial \bar{v}}{\partial t} + \nabla \bar{v}\bar{v}\right) = -\nabla \bar{p} + \nabla \cdot \mu \cdot (\nabla \bar{v} + \nabla \bar{v}^T) \tag{14}$$

This equation is more complex than that following the Navier Stokes formulation due to discontinuities in density and viscosity and the insertion of the interface boundary conditions, that in their integral form are (Graveleau 2016):

$$F_{sb} = \frac{1}{V}\int_{A_{sb}} [-\rho_s(v_s - \boldsymbol{v})v_s - Ip_s + \mu_s(\nabla v_s + (\nabla v_s)^T)]\, \boldsymbol{n}_{sb} dA \tag{15}$$

$$F_{bs} = \frac{1}{V}\int_{A_{bs}} [-\rho_b(v_b - \boldsymbol{v})v_b - Ip_b + \mu_b(\nabla v_b + (\nabla v_b)^T)]\boldsymbol{n}_{bs} dA \tag{16}$$

According to the force equilibrium boundary condition, it derives to:

$$F_{sb} + F_{bs} = F_c = \frac{1}{V}\int_{A_{sb}} \sigma H_{sb}\, \boldsymbol{n}_{sb} dA \tag{17}$$

Therefore, under the one fluid approach, the momentum equation becomes:

$$\rho\left(\frac{\partial \bar{v}}{\partial t} + \nabla \bar{v}\bar{v}\right) = -\nabla \bar{p} + \nabla \cdot \mu \cdot (\nabla \bar{v} + \nabla \bar{v}^T) + F_c \tag{18}$$

In order to compute the interfacial forces (F_c), the Continuum Surface Force model (CSF) proposed by Brackbill (Brackbill, Kothe, and Zemach 1992) is considered.

This method allows representing the surface tension, by nature a surface force, as a volumetric contribution acting on the region where the interface lies, in accordance with the VOF method through the indicator function:

$$F_c = \sigma \nabla \cdot \left(\frac{\nabla \alpha}{|\nabla \alpha|}\right) \nabla \alpha \tag{19}$$

This set of equations is the basis to simulate the interfacial mass transfer physics under the VOF approach.

2.4. Interfacial diffusion approach

Interfacial diffusion is a physical phenomenon linked to the solvent injection process for heavy oil recovery. Usually, experimental studies about this topic may be not only elaborate and time consuming, but also unable to access to local fluid dynamics and isolated mechanisms controlling it. Direct numerical simulations aided by the VOF approach allow describing these mechanisms at the interface level.

For this purpose, a set of equations is derived from the Navier-Stokes and species conservation equations, and their variables described by the volume fraction indicator, α, representing the presence of each phase. Starting from the conservation equations for local species, j, within each bulk phase that read as:

Solvent (s)

$$\frac{\partial C_{j,s}}{\partial t} + \nabla \cdot \left[u_s C_{j,s}\right] = -\nabla\left(D_{js} \nabla C_{js}\right) + W_{j,s} \tag{20}$$

Bitumen (b)

$$\frac{\partial C_{j,b}}{\partial t} + \nabla \cdot \left[u_b C_{j,b}\right] = -\nabla\left(D_{jb} \nabla C_{jb}\right) + W_{j,b} \tag{21}$$

Where $C_{j,s/b}$, $D_{j,s/b}$ and $W_{j,s/}$ stand for concentration, diffusion coefficient and production/consumption rate by chemical reaction of species j in each phase, which boundary conditions at interface are:

$$C_{j,b} He_j = C_{j,s} \tag{22}$$

It represents the solubility of chemical species, which physically refers to the species j concentration in bitumen when it is at thermodynamic equilibrium with solvent, for a given pressure and temperature.

Equation (23), on the other hand, describes the sum of diffusive molecular fluxes across the interface in both directions, where no material accumulation occurs due to fluxes continuity (Haroun 2008).

$$\sum_K J_{j,K} = 0 \tag{23}$$

$$J_{j,K} = -D_{j,K}\nabla C_{j,K} \tag{24}$$

$$K = Solvent\ or\ Bitumen$$

Where J is the species diffusive flux of the species K .

In accordance to the one-fluid approach described in the previous section, the species concentration conservation equations must be formulated as a single expression valid in the entire domain. In consequence, equations (20) and (21) are multiplied by the volume fraction indicator, α, and summed up to describe the two phases as a mixture:

$$\frac{\partial}{\partial t}\left[\sum_K \alpha_K C_K\right] + \nabla \cdot \left[\sum_K \alpha_K C_K u_K\right] = -\nabla \cdot \left[\sum_K \alpha_K J_K\right] + \sum_K \alpha_K W_K \tag{25}$$

$$K = Solvent\ or\ Bitumen$$

This mixture description relies on mixture variables, which definition for concentration and diffusion coefficient are respectively:

$$C_j = \alpha C_j^b + (1-\alpha) C_j^s \tag{26}$$

$$D_j = \alpha D_j^b + (1-\alpha) D_j^s \tag{27}$$

Replacing the concentration for its mixture definition (26) and removing the chemical reaction term in (25), it reads:

$$\frac{\partial C_j}{\partial t} + \nabla \cdot u C_j = -\nabla \cdot \left[\sum_K \alpha_K J_K\right] \tag{28}$$

The chemical reaction term is eliminated because it is not in the scope of the physics being modeled in this thesis. According to the diffusive molecular flux definition, the RHS of (28) can be written as follows:

$$\frac{\partial C_j}{\partial t} + \nabla \cdot uC_j = -\nabla \cdot \left[-D \left(\nabla C - \sum_K C_K \cdot \nabla \alpha \right) \right]$$

$$\frac{\partial C_j}{\partial t} + \nabla \cdot uC_j = \nabla D \nabla C - D \sum_K C_K \nabla \alpha \tag{29}$$

Equation (29) differs from the conventional advection-diffusion equations describing concentration in the bulk phases by the last term on the RHS. This term comes from the one-fluid derivation and corresponds to an additional flux occurring at the interface. It allows representing the concentration discontinuity at the interface in terms of Henry's relation and mixture concentration:

$$\emptyset = -D \sum_K C_K \nabla \alpha = -D \left[\frac{C_j (1 - He)}{\alpha + He(1 - \alpha)} \nabla \alpha \right] \tag{30}$$

This term is only valid in the interfacial region where $\nabla \alpha \neq 0$ and becomes zero for $He = 1$. In this case, the concentration evolution at the interface is continuous. This equation is valid in the entire computational domain, and its final form reads (Haroun 2008):

$$\frac{\partial C_j}{\partial t} + \nabla \cdot uC_j = \nabla D_j \nabla C - D_j \left[\frac{C_j (1 - He)}{\alpha + He(1 - \alpha)} \nabla \alpha \right] \tag{31}$$

2.5. DIFFUSION COEFFICIENT

The method presented here can simulate the diffusion process under the VOF framework. However, it does not account for the diffusivity concentration dependence. In this work, this feature is added to the solver governing equations by means of models derived from experimental results. This addition is further explained in Chapter 4.

In this chapter, two simulation cases representing the diffusion process occurring in systems with different characteristics are presented. These digital representations are intended to assess the capability of the model to accurately reproduce the physics of the process.

The first case is referred to as Case 1. It represents a system where, at one of the boundaries, species concentration is kept constant while it diffuses over a medium with zero initial concentration. In this exercise, the grid refinement effect on the accuracy of the results and computational cost are evaluated. Furthermore, the model capability to handle representative diffusivities is verified.

With a length of 0.01 m in x and y directions, the computational model used to simulate one-dimensional diffusion in a semi-infinite medium is shown in Figure 3.1.

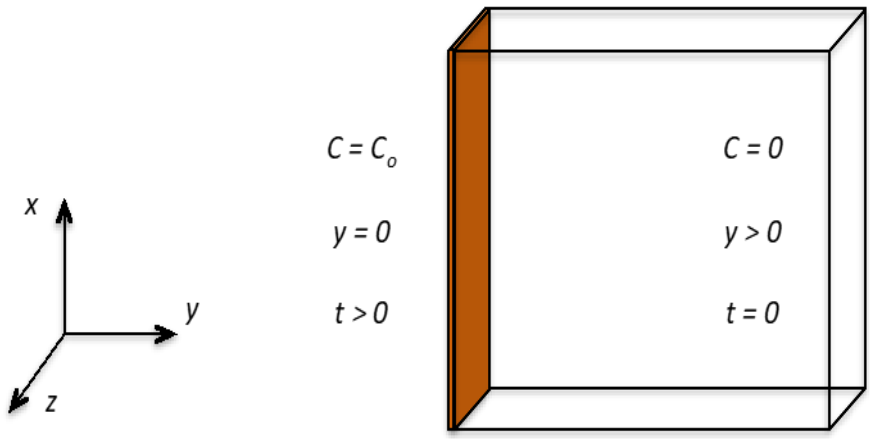

Figure 3.1 One-dimension diffusion.

The species concentration evolution as function of time and position are described by the equation:

$$\frac{\partial C}{\partial t} = D\frac{\partial^2 C}{\partial y^2} \tag{32}$$

The solution that satisfies the initial and boundary conditions described in Figure 3.1 is written as (Crank 1979):

$$C = C_o erfc\left(\frac{y}{2\sqrt{Dt}}\right) \tag{33}$$

3.1. GRID REFINEMENT EFFECT.

For numerical approaches, not only the solver, but also the grid refinement plays an important role in generating accurate results. This accuracy is primarily measured relative to highly accurate solutions like the analytical ones.

In order to determine the effect of grid refinement on numerical results, concentration data in different grids are computed. Afterwards, these are compared to those from the analytical solution in Figure 3.2.

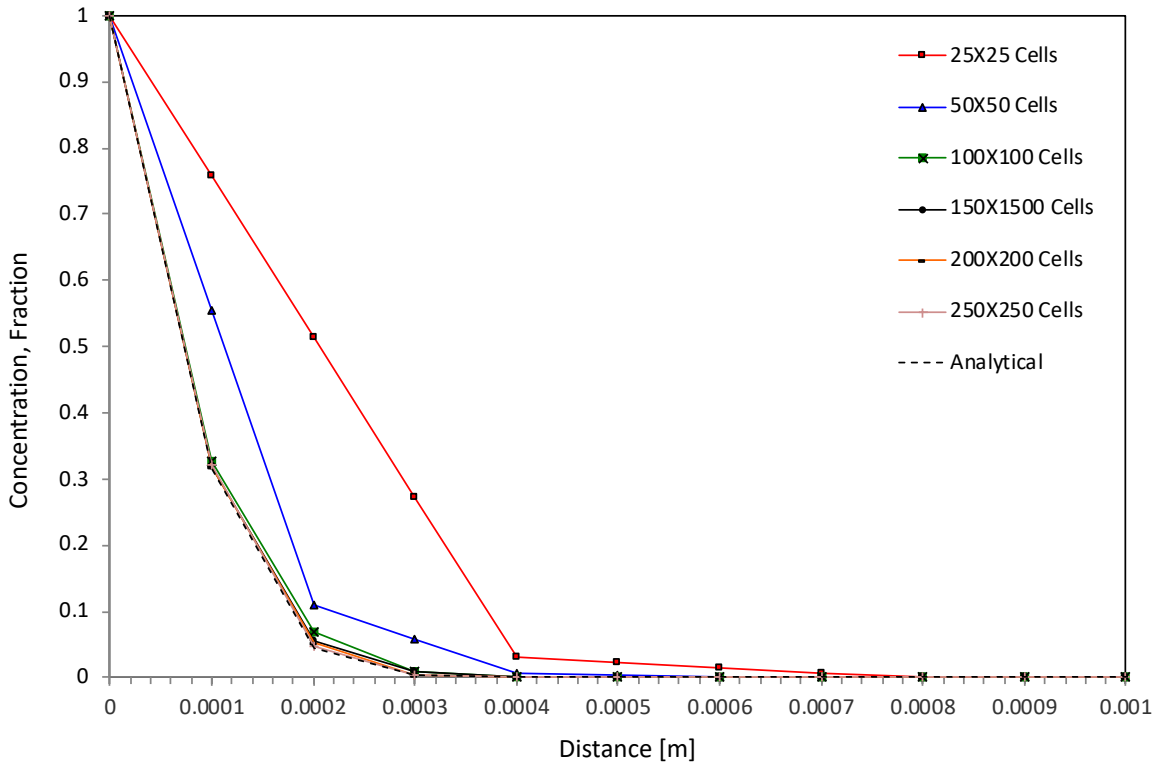

Figure 3.2 Grid refinement effect ($D = 1E-9\ m^2/s, t = 5s$).

It can be seen in Figure 3.2, that as the grid refinement increases, the agreement between numerical and analytical solutions improves. From these results, the absolute error between numerical and analytical solutions is computed through the expression below:

$$\varepsilon_a = \sum (X_A - X_N)^2 \tag{34}$$

X_A and X_N are the analytical and numerical values respectively.

In Figure 3.3, the absolute error and simulation time are plotted against the number of cells. It can be inferred from the graph that an inversely proportional relationship exists between

the accuracy and simulation time spent, which depends on the available computational resource.

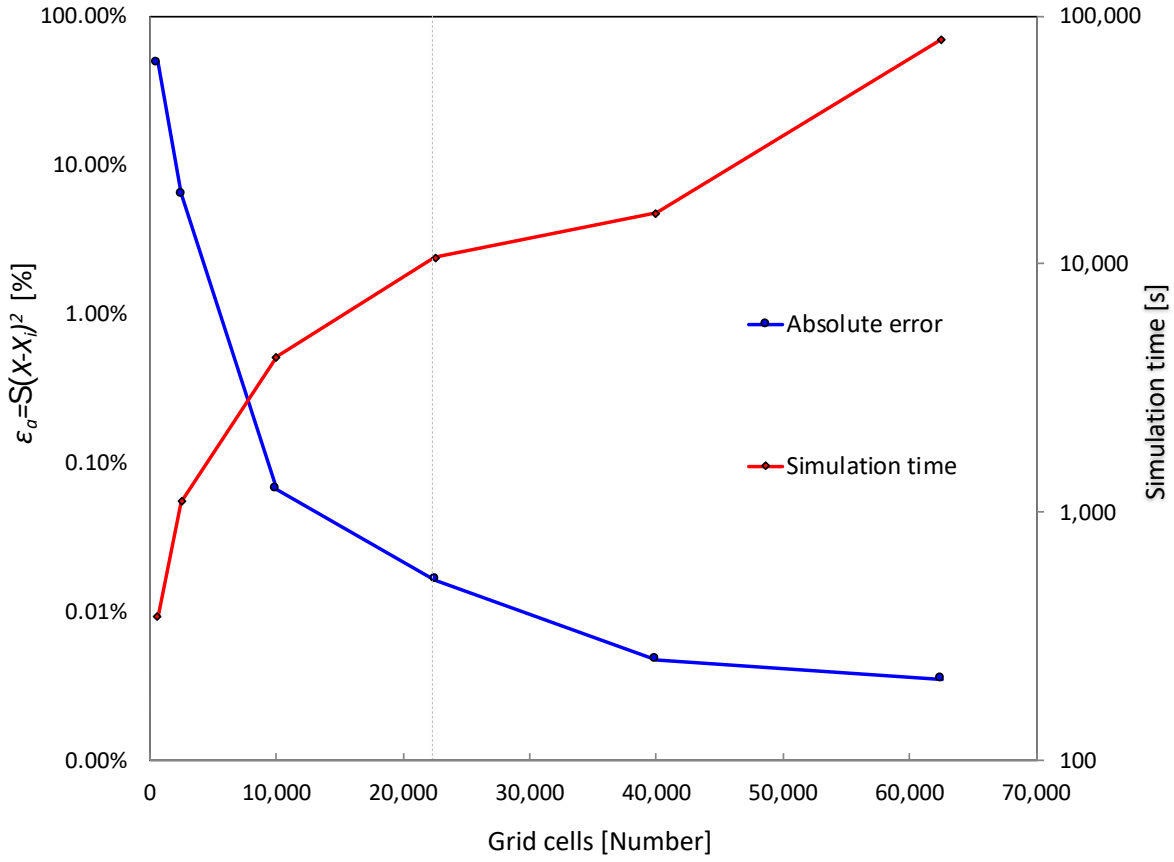

Figure 3.3 Grid cells test ($D = 1E-9\ m^2/s, t = 5s$).

As observed in Figure 3.3, an increase in accuracy is obtained as the number of grid-cells increases. Nevertheless, after ~22,500 grid cells, start to define a plateau and the gain in accuracy is not significant after this point.

To better visualize this behaviour, the data displayed in Figure 3.3 is summarized in Table 3.1 including also the cell size for each case.

Table 3.1 Diffusivity range evaluation

Number of cells	Cell size [m]	Simulation time [s]	Absolute error [%]
625	1.60E-05	381	48.9046
2,500	4.00E-06	1,106	6.4172
10,000	1.00E-06	4,219	0.0670
22,500	4.44E-07	10,643	0.0165
40,000	2.50E-07	16,029	0.0048
62,500	1.60E-07	80,137	0.0035

From the previous analysis, it can be concluded that the selection of number of grid cells depends on the accuracy required to obtain representative results, which is limited only by the computational power and time available. For the simulation results presented in this thesis, a cells size on the order of micrometers was used as the minimum required, since it gives a suitable accuracy with the lowest computational cost.

3.2. DIFFUSIVITY RANGE

The following simulations are intended to evaluate the model capability to handle diffusivities in the range $1E-5$ to $1E-11\ m^2/s$, which are expected for the systems studied in this work (Guerrero-Aconcha 2009; Wen and Kantzas 2005).

Concentration profiles are simulated during time scales that allow the diffusion process to occur, and then they are compared to results from analytical solutions in Figures 3.4 to 3.7.

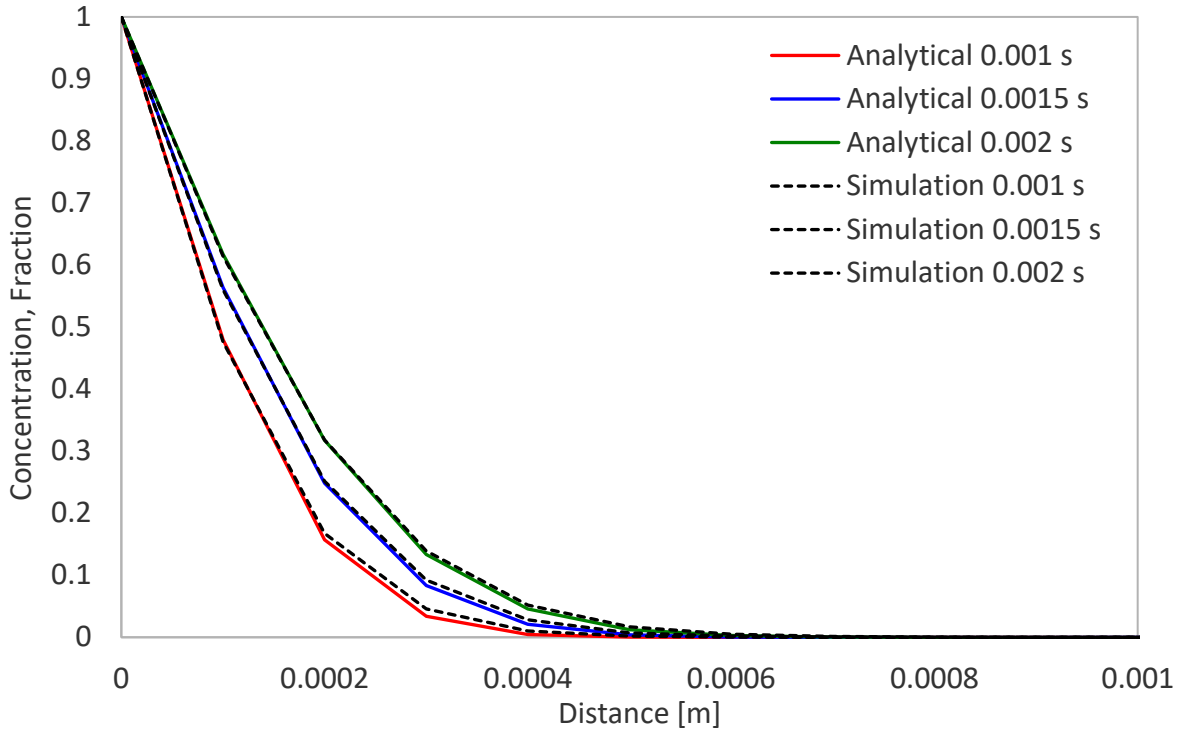

Figure 3.4 Concentration profiles, ($D = 1E-5\ m^2/s$).

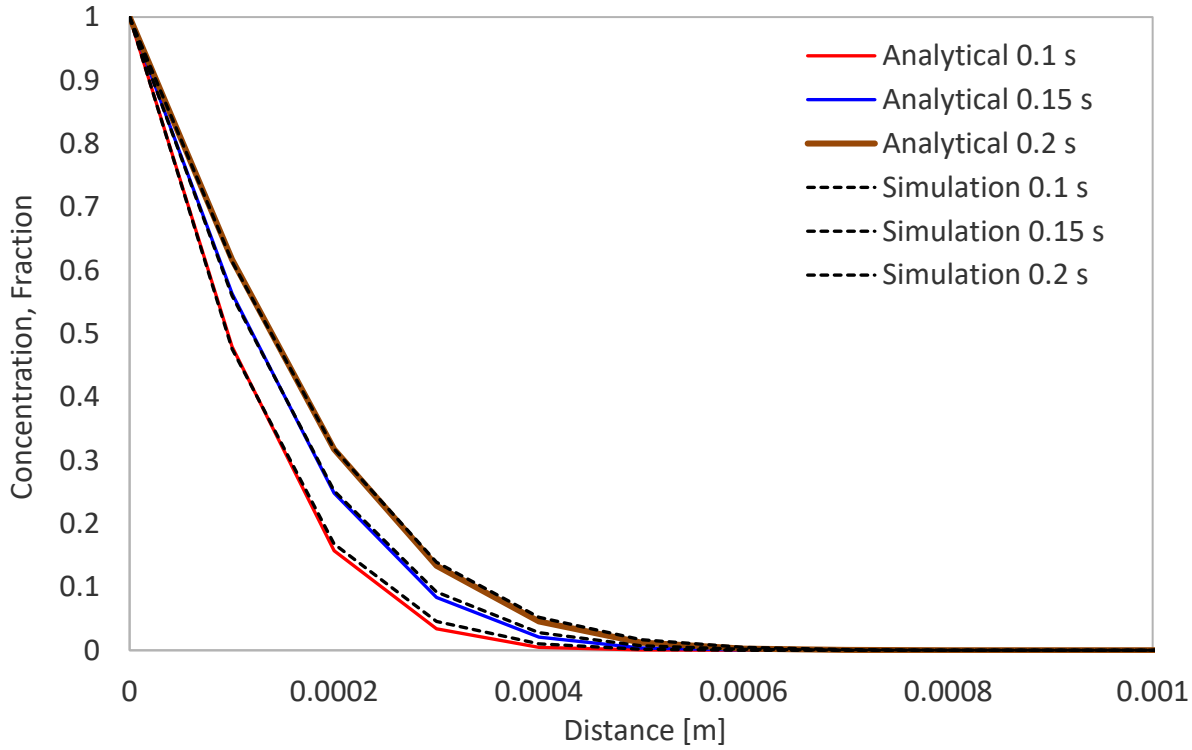

Figure 3.5 Concentration profiles, ($\mathrm{D} = 1\mathrm{E}-7\ \mathrm{m}^2/\mathrm{s}$).

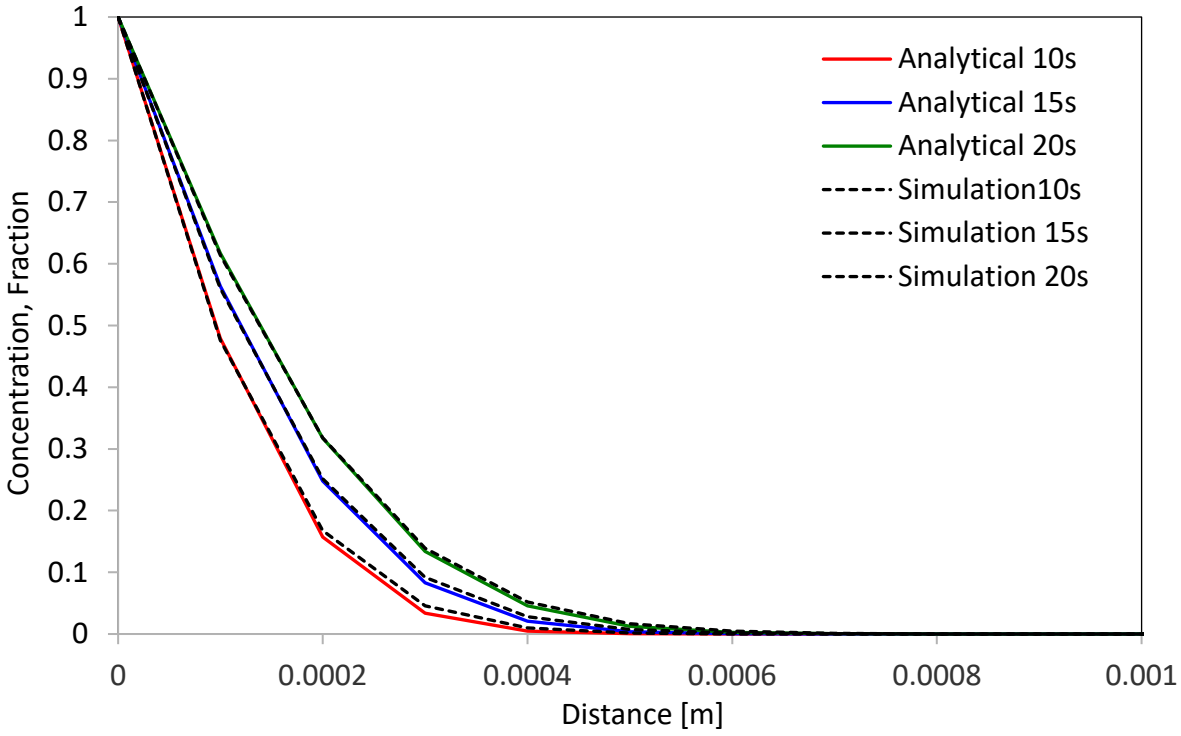

Figure 3.6 Concentration profiles, ($\mathbf{D = 1E-9\ m^2/s}$).

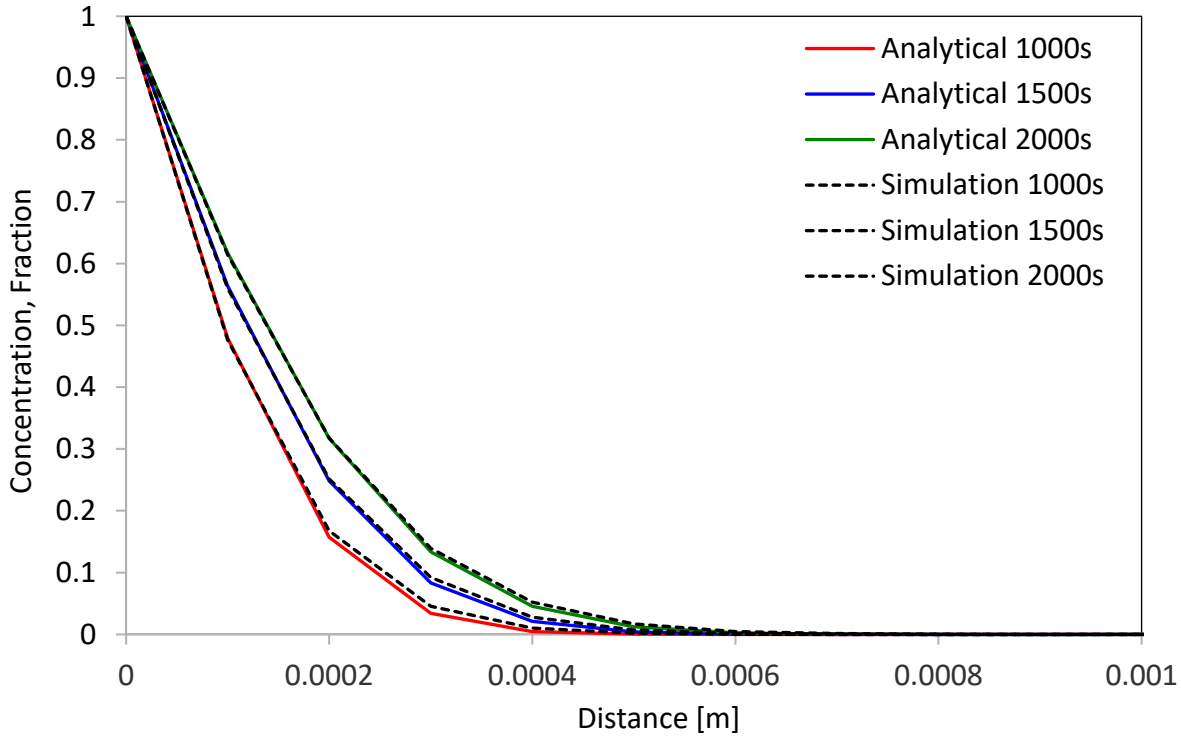

Figure 3.7 Concentration profile, ($\mathbf{D = 1E-11\ m^2/s}$).

From Figures 3.4 to 3.7, it can be concluded that for the whole range of diffusivities there is a good agreement between simulated and analytical data. Table 3.2 summarizes the ranges of absolute error between them.

Table 3.2 Diffusivity range evaluation

Case	Diffusivity [m^2/s]	Simulation time [s]	Absolute error [%]
1	1E-5	0.0010, 0.0015, 0.0020	0.0290, 0.0163, 0.0107
	1E-7	0.10, 0.15, 0.20	0.0289, 0.0162, 0.0106
	1E-9	10, 15, 20	0.0289, 0.0163, 0.0106
	1E-11	1000, 1500, 2000	0.0289, 0.0163, 0.0107

The grid cells size chosen lead to a smaller deviation than the observed in previous analysis for the same grid cell size. This result confirms the model capability to simulate physical processes occurring in this range.

3.3. INTERFACIAL MASS TRANSFER

In Case 2, a system where species at a uniform concentration in one fluid diffuses to other through an interface is presented. Here, the capability of the simulation model to handle the properties discontinuity at the interface is assessed.

The test is conducted in a computational domain with 0.01 m length in x and y directions as shown in Figure 3.8.

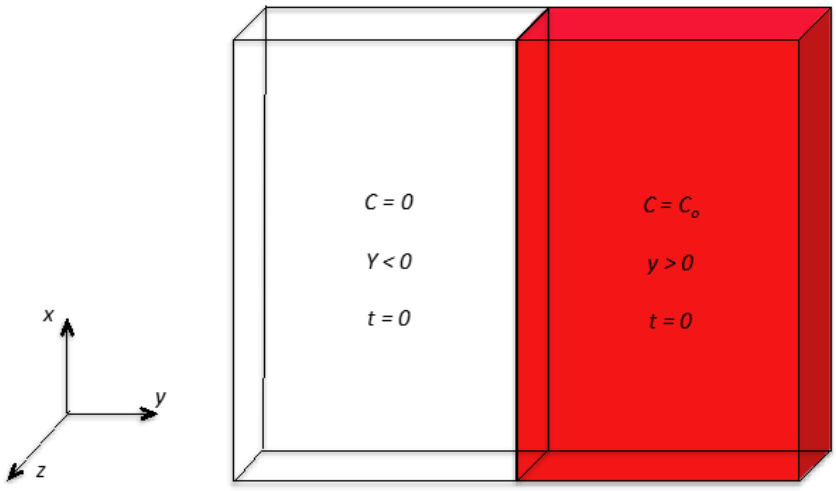

Figure 3.8 Infinite composite medium.

The species concentration evolution as a function of time and position for an *infinite composite medium* is described by the equation:

$$\frac{\partial C}{\partial t} = D\frac{\partial^2 C}{\partial y^2} \tag{35}$$

Each fluid in the system has a uniform diffusion coefficient and initial concentrations as showed in Figure 3.8. Concentration at right and left sides of the interface are $C_o = C_1 = 1$, and $C = C_2 = 0$ respectively. Thus, the following conditions at the interface can be applied.

$$C_1/C_2 = He, \qquad y = 0 \tag{36}$$

$$D_1\frac{\partial C_1}{\partial y} = D_2\frac{\partial C_2}{\partial y}, \qquad y = 0 \tag{37}$$

The analytical solution satisfying the initial and boundary conditions in Figure 3.8 is written as (Crank 1979):

$$C_1 = \frac{C_o}{1 + He(D_2/D_1)^{\frac{1}{2}}}\left[1 + He(D_2/D_1)^{\frac{1}{2}} erf\frac{y}{2\sqrt{D_1 t}}\right], \qquad y > 0 \tag{38}$$

$$C_2 = \frac{HeC_o}{1 + He(D_2/D_1)^{\frac{1}{2}}} erfc\frac{|y|}{2\sqrt{D_2 t}}, \qquad y < 0 \tag{39}$$

On the other hand, the numerical solution follows the VOF approach. This methodology relies on the Henry's law constant to describe the species concentration discontinuity at the interface (Deising, Marschall, and Bothe 2016). When the equations are discretized, an interface digital thickness is induced to continuously describe magnitudes of both phases (Haroun 2008). Different from the rest of the computational domain where the volume fraction is computed in several discrete points, the digitally spread interface representation, provides an average volume of concentration only in the cells containing the interface. Thus, the sharpness of the digital interface will be defined by how much the grid can be refined. An example of this representation is showed in Figure 3.9.

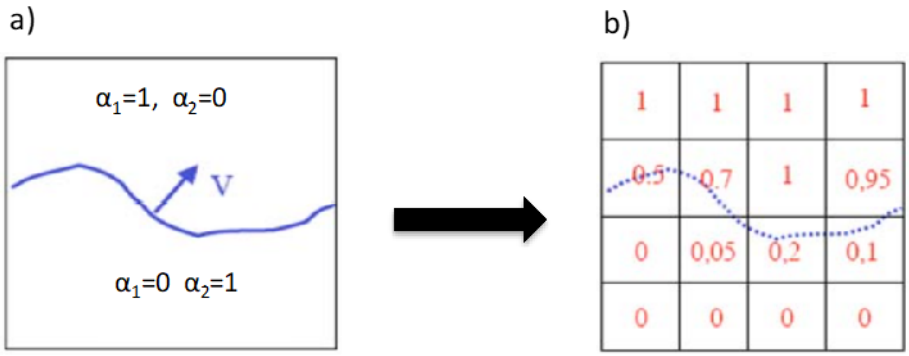

Figure 3.9 Two phases numerical description. a) Indicator phase function, b) Average volume of the magnitude in the cell (Haroun 2008)**.**

Concentration profiles for $D = 1E-7\ m^2/s$ and $He = 5$ are simulated for $0.2\ s$ in meshes with different grid cell sizes. In Figure 3.10, these results are compared to the analytical ones to show the effect on the interphase representation.

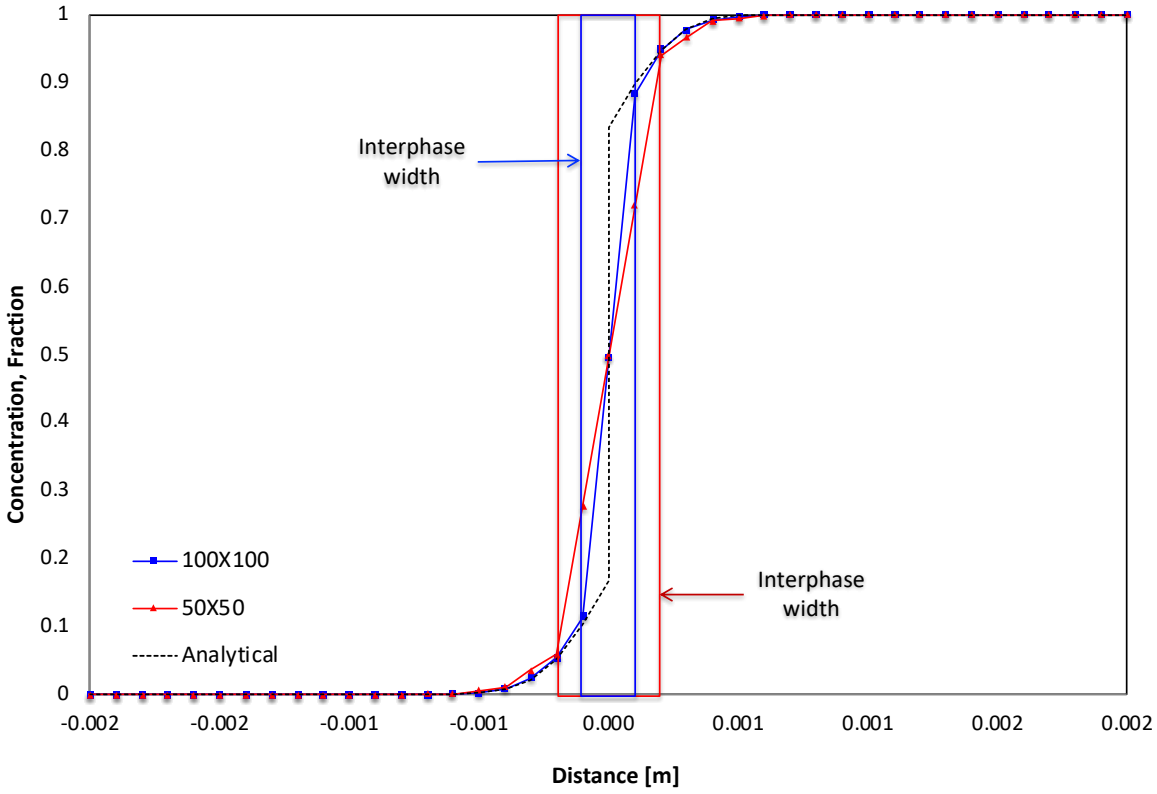

Figure 3.10 Interphase digital representation.

It can be observed that the number of cells defined in the interfacial region determines the interphase thickness. This local refinement leads to interfacial numerical descriptions closer to the analytical ones.

A common problem when simulating two-phase systems at small scales is the artificial velocities appearing at the interface (Haroun 2008). The origin of this numerical artifact is the unbalance between discrete representations of forces across the interface (Santiago 2015).

For the system simulated in Case 2, both fluids are physically stationary. However, the numerical solution of the concentration conservation equation (40), yields a general velocity field where both fluids are not at rest.

$$\frac{\partial C}{\partial t} + \nabla \cdot (uC) = -\nabla D \nabla C + W \tag{40}$$

Therefore, artificial velocities occur in the neighbourhood of the interface.

In order to avoid the artificial velocities incidence, static conditions are assumed. The numerical solver is configured to solve the equation (40) with (dynamic conditions) and without (static conditions) the second term in the LHS. Then, both simulations results are compared. These assumptions are valid if molecular diffusion occurs between liquids. Concentration profiles for the whole range of diffusivities are showed in Figures 3.11 to 3.14.

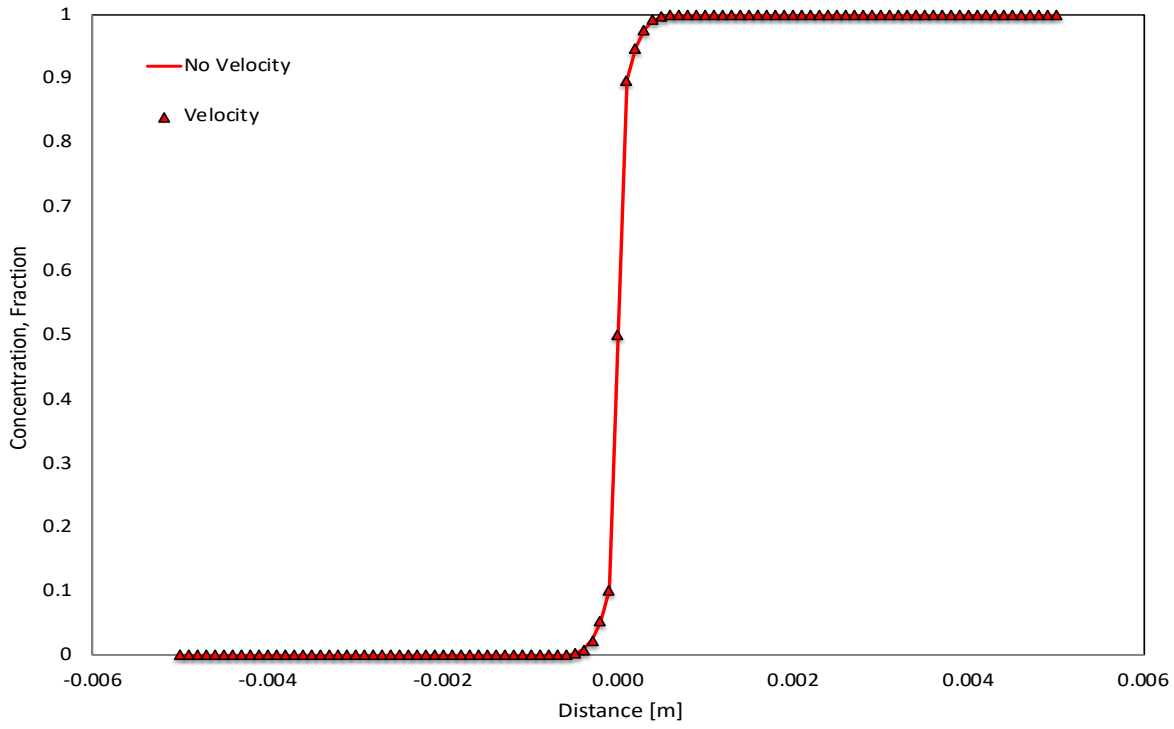

Figure 3.11 $D1 = D2 = 1E-5\ m^2/s, t = 0.002\ s$.

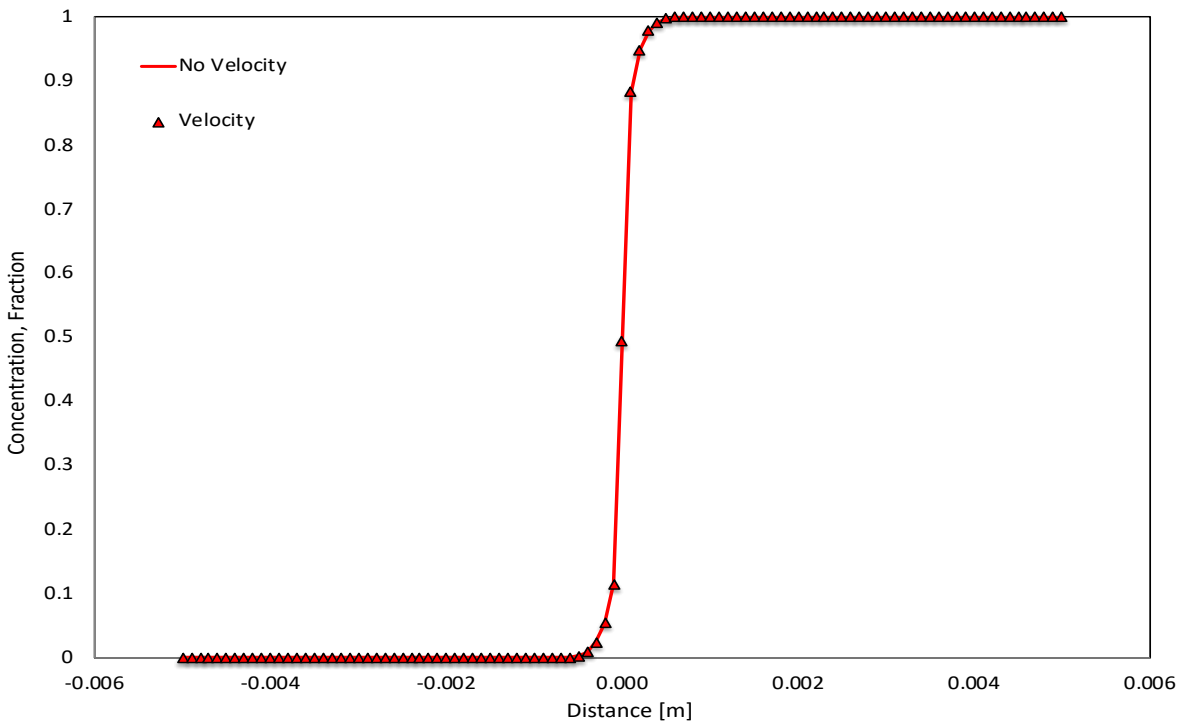

Figure 3.12 $D1 = D2 = 1E-7\ m^2/s,\ t = 0.2\ s.$

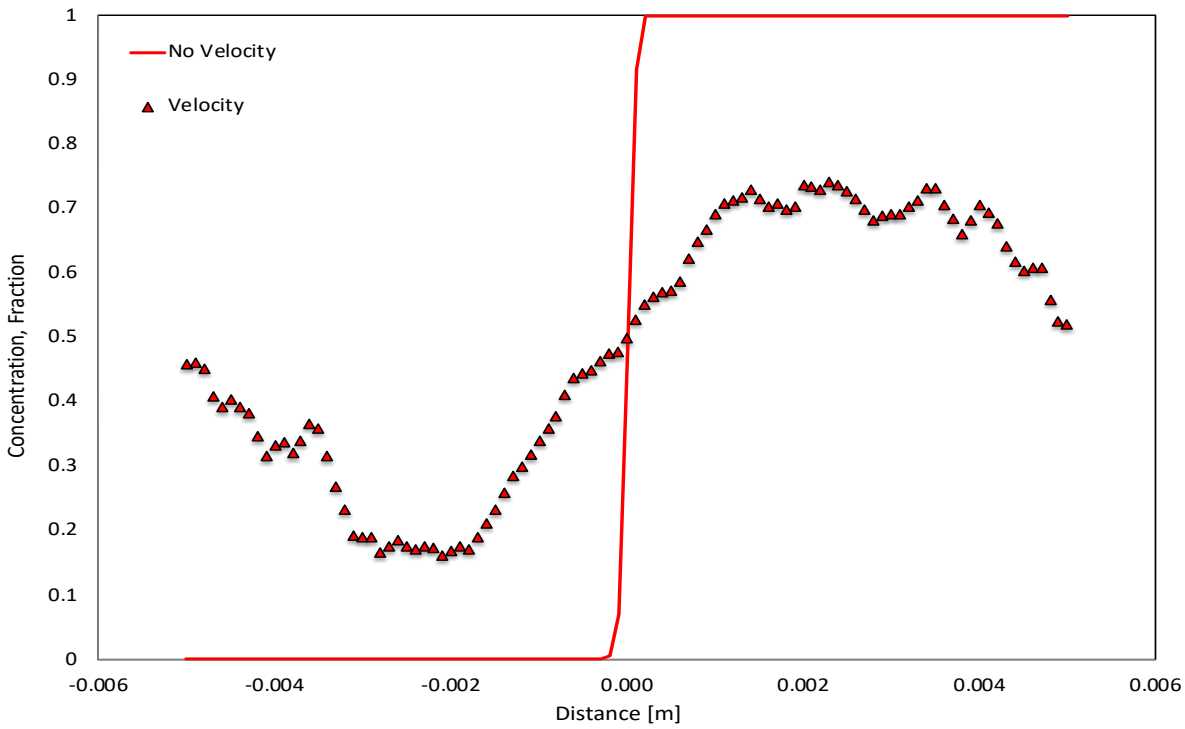

Figure 3.13 $D1 = D2 = 1E-9\ m^2/s,\ t = 20\ s.$

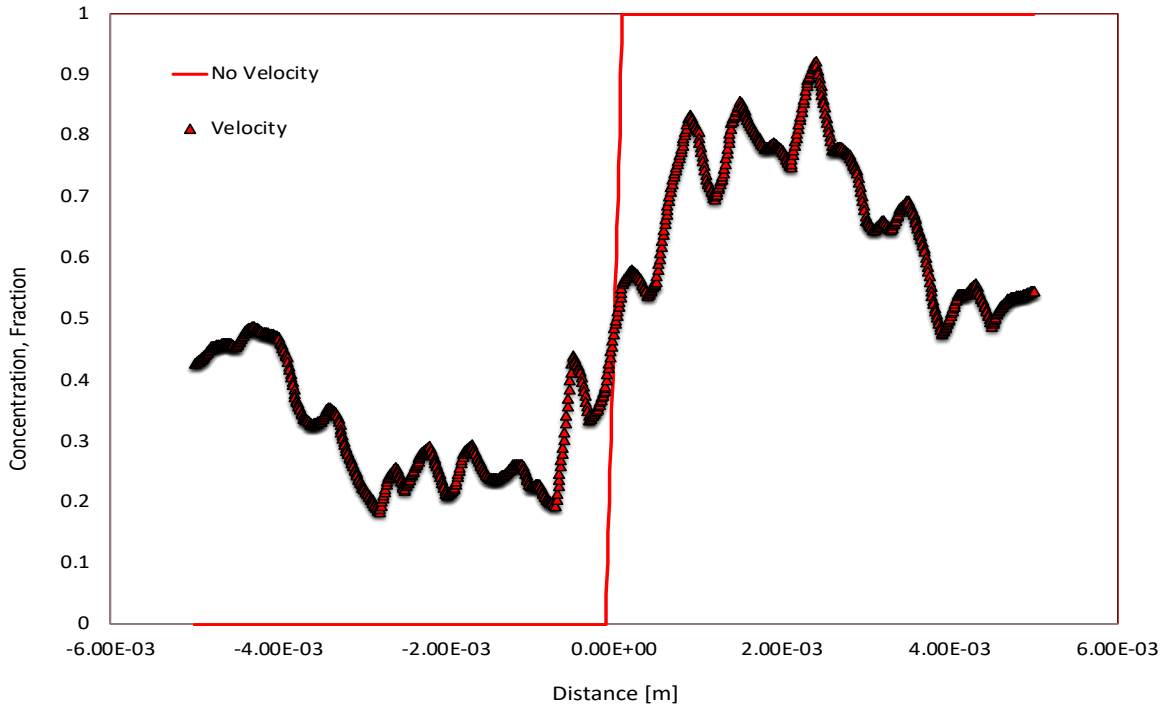

Figure 3.14 $D1 = D2 = 1E-11\ m^2/s,\ t = 2000\ s$.

It can be seen in Figures 3.11 and 3.12 that for the upper range limit of diffusivities, the concentration field shows an expected physical behaviour. In this case, the diffusive flux compensates concentration variations due convection.

For lower diffusivities (Figures 3.13 and 3.14), on the other hand, any velocity peak will cause the appearance of artificial velocities.

This effect can be explained by comparing the convective and diffusive terms in the Table 3.3., which magnitudes can be estimated from the maximum velocity field, diffusion coefficient and cell´s characteristic length, through the following equation.

$$\frac{1}{L}\cdot(UC) \approx \frac{1}{L}\cdot\left(D\frac{1}{L}C\right) \tag{41}$$

Table 3.3 Convective and diffusive fluxes effect.

Average maximum velocity [m/s]	D [m^2/s]	Cell size [m]	Convective flux [1/s]	Diffusive flux [1/s]
2.85E-03	1.00E-05	1.00E-06	2.85E+03	1.00E+07
3.70E-05	1.00E-07		3.70E+01	1.00E+05
1.28E-01	1.00E-09		1.28E+05	1.00E+03
9.22E-01	1.00E-11		9.22E+05	1.00E+01

The results in Table 3.3 show that if dynamic conditions are considered, convective flux becomes around two orders of magnitude bigger than the diffusive one. This sharp increase leads to an unbalance that originates unphysical results.

An additional case involving two different fluids is evaluated. Except by the diffusivities of the fluids ($D_1 = 1E-7, D_2 = 1E-6\ m^2/s$), dimensions, initial and boundary conditions are the same as previous example. Simulations are run for $He = 5$ and different simulation times. The results are compared to analytical results in Figure 3.15.

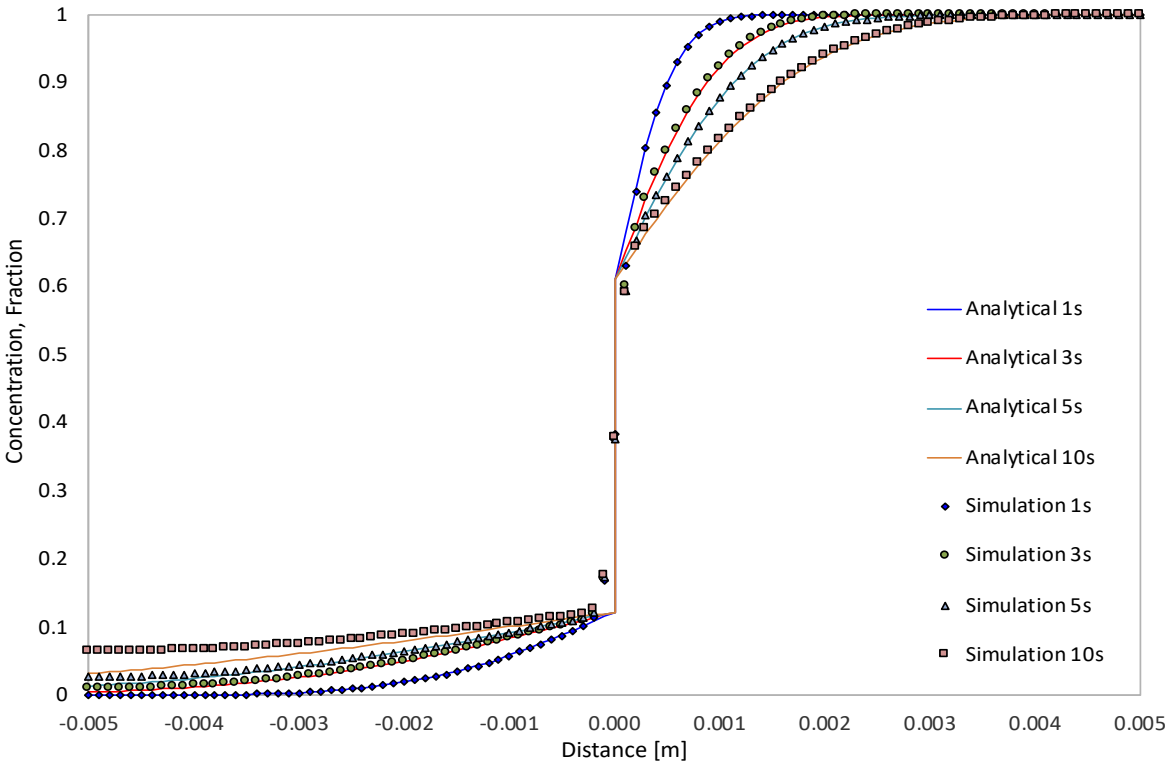

Figure 3.15 concentration profiles $(\boldsymbol{D1 = 1E-7, D2 = 1E-6\ m^2/s})$ **.**

Results in Figure 3.15 demonstrate that the simulation model can reproduce mass transfer between fluids with different diffusivities if the convective term in the concentration conservation equation is removed.

CHAPTER 4. CONCENTRATION DEPENDENT MASS TRANSFER SIMULATIONS.

Once the original *interFoam* solver was enabled to handle interfacial diffusion, it was modified to account for diffusion coefficient dependence on solvent concentration. To do so, two approaches were followed.

4.1. SLOPES AND INTERCEPTS MODEL

Proposed by Sarafianos (Sarafianos 1986) and generally referred as the Slopes and Intercepts method (S&I), this analytical approach estimates mutual diffusion coefficients for the whole fluids concentration range in a binary system. This technique was employed by Guerrero (Guerrero-Aconcha 2009) to calculate diffusion coefficients from data of solvent concentration in heavy oil. The diffusion coefficients obtained were fitted to polynomial relations to describe them as function of concentration, Figure 4.1.

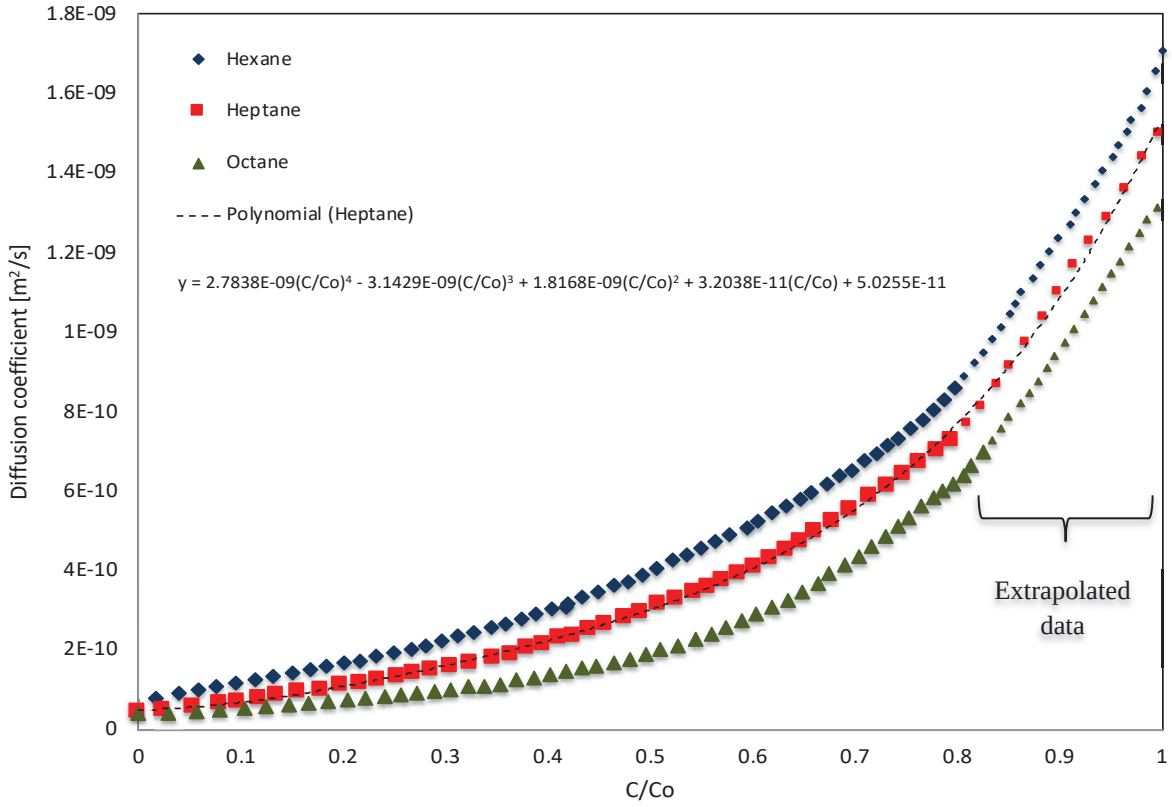

Figure 4.1 Diffusion coefficient for n-hexane, n-heptane and n-octane in heavy oil at 25℃, Slopes and Intercepts (Guerrero-Aconcha 2009)**.**

The Concentration Dependent Diffusion Polynomial (CDDP) fitted to the results obtained by Guerrero, was then implemented in the *interFoam* solver to calculate updated diffusion coefficients for each time step to solve the concentration field.

4.2. VIGNES MODIFIED MODEL

The Vignes model (Vignes 1966) is an empirical correlation based on experimental results that predicts the mutual diffusion coefficient as a function of the solution composition.

It depends on diffusion coefficients at infinite dilution, mole fraction of the components of the solution and thermodynamic activities as entry data. These thermodynamic parameters represent the solution deviation from ideality. However, they are empirically assumed due its difficulty to be obtained, leading to uncertain diffusion coefficient estimations (Guerrero-Aconcha 2009).

To overcome this uncertainty, Mendoza et al. (Mendoza, Babak, and Kantzas 2018) proposed a modification of the Vignes methodology (VM), where 'acceleration' and 'deceleration' parameters, associated to solvent and solute mass transfer behaviour, are included in the following form of the Vignes equation.

$$D_{ij} = \left(D_{ij}^{\infty}\right)^{c_j\left(1+\delta c_i c_j\right)}\left(D_{ji}^{\infty}\right)^{c_i\left(1+\beta c_i c_j\right)} \tag{42}$$

By adjusting a second order polynomial to the deviation of Vignes from the Slope and Intercepts diffusion estimations, the correction parameters are determined by means of a regression. This methodology was employed to reproduce the diffusion coefficients previously estimated by (Guerrero-Aconcha 2009), through the Slopes and Intercepts method.

The 'acceleration' and 'deceleration' parameters estimated through the Mendoza's et al (Mendoza, Babak, and Kantzas 2018) methodology, to fit the Slopes and Intercepts diffusion coefficient profiles in figure 4.2, are presented in the table below.

Table 4.1 Vignes Modified model 'acceleration' and 'deceleration' parameters.

	δ	β
Hexane	-0.1278	0.0819
Heptane	-0.1921	-0.0315
Octane	-0.0151	-0.1069

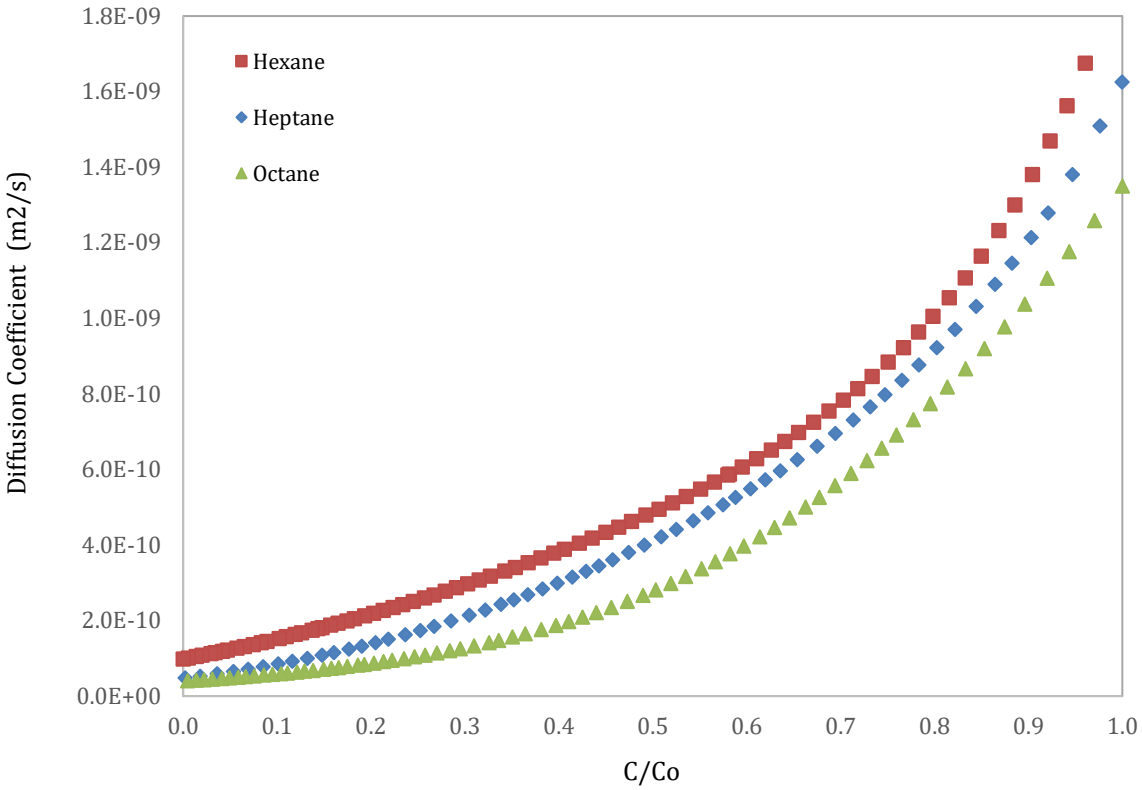

Figure 4.2 Diffusion coefficient for n-hexane, n-heptane and n-octane in heavy oil at 25℃, Vignes Modified.

The Vignes Modified model and the polynomial relations from the slopes and intercepts method were also implemented in the *interFoam* solver. Thus, with the addition of the interfacial and concentration dependent diffusion features, a new solver has been developed.

In this chapter, experimental measurements conducted by Salama (Salama 2006) and Diedro (Diedro et al. 2015) are simulated to verify the accuracy of the developed model.

The experiments consisted on measuring properties of the fluids in solvent-heavy oil and solvent-bitumen systems by using Computer Assisted Tomography (CAT) (Kantzas 1990). Measurements were translated into density and solvent concentration profiles.

Since X-rays attenuation is a linear function of bulk density (Kantzas 1994), samples of known densities were scanned and then correlated to CT numbers readings. From these correlations solvent-bitumen and solvent-heavy oil mixture densities were obtained, and subsequently translated to concentration data through the following equation, in (Salama 2006) and (Guerrero-Aconcha 2009):

$$C_S = \frac{\rho_{mix} - \rho_B}{\rho_S - \rho_B} \tag{43}$$

An example of the concentration profile estimation for the hexane – heavy oil system, is presented in the following table.

Table 4.2 Hexane system concentration profile data.

	ρ_B (g/cm^3)	ρ_S (g/cm^3)	ρ_{mix} (g/cm^3)	C_S $(fraction)$		ρ_B (g/cm^3)	ρ_S (g/cm^3)	ρ_{mix} (g/cm^3)	C_S $(fraction)$
1	0.9780	0.6650	0.6650	1.0000	39	0.9780	0.6650	0.7964	0.5803
2	0.9780	0.6650	0.6650	0.9999	40	0.9780	0.6650	0.8071	0.5459
3	0.9780	0.6650	0.6651	0.9998	41	0.9780	0.6650	0.8209	0.5019
4	0.9780	0.6650	0.6651	0.9996	42	0.9780	0.6650	0.8290	0.4760
5	0.9780	0.6650	0.6655	0.9985	43	0.9780	0.6650	0.8377	0.4483
6	0.9780	0.6650	0.6655	0.9984	44	0.9780	0.6650	0.8446	0.4263
7	0.9780	0.6650	0.6655	0.9982	45	0.9780	0.6650	0.8530	0.3995
8	0.9780	0.6650	0.6656	0.9981	46	0.9780	0.6650	0.8616	0.3718
9	0.9780	0.6650	0.6659	0.9970	47	0.9780	0.6650	0.8694	0.3469
10	0.9780	0.6650	0.6660	0.9969	48	0.9780	0.6650	0.8802	0.3125
11	0.9780	0.6650	0.6660	0.9968	49	0.9780	0.6650	0.8886	0.2857
12	0.9780	0.6650	0.6666	0.9948	50	0.9780	0.6650	0.8982	0.2551
13	0.9780	0.6650	0.6667	0.9946	51	0.9780	0.6650	0.9077	0.2244
14	0.9780	0.6650	0.6661	0.9964	52	0.9780	0.6650	0.9161	0.1977
15	0.9780	0.6650	0.6668	0.9944	53	0.9780	0.6650	0.9251	0.1690
16	0.9780	0.6650	0.6674	0.9923	54	0.9780	0.6650	0.9353	0.1364
17	0.9780	0.6650	0.6686	0.9884	55	0.9780	0.6650	0.9455	0.1039
18	0.9780	0.6650	0.6705	0.9825	56	0.9780	0.6650	0.9524	0.0819
19	0.9780	0.6650	0.6735	0.9729	57	0.9780	0.6650	0.9596	0.0589
20	0.9780	0.6650	0.6765	0.9632	58	0.9780	0.6650	0.9635	0.0465
21	0.9780	0.6650	0.6804	0.9507	59	0.9780	0.6650	0.9683	0.0311
22	0.9780	0.6650	0.6849	0.9363	60	0.9780	0.6650	0.9716	0.0205
23	0.9780	0.6650	0.6900	0.9200	61	0.9780	0.6650	0.9743	0.0118
24	0.9780	0.6650	0.6939	0.9075	62	0.9780	0.6650	0.9752	0.0089
25	0.9780	0.6650	0.6993	0.8903	63	0.9780	0.6650	0.9762	0.0059
26	0.9780	0.6650	0.7053	0.8711	64	0.9780	0.6650	0.9768	0.0038
27	0.9780	0.6650	0.7116	0.8510	65	0.9780	0.6650	0.9766	0.0046
28	0.9780	0.6650	0.7176	0.8319	66	0.9780	0.6650	0.9766	0.0044
29	0.9780	0.6650	0.7227	0.8156	67	0.9780	0.6650	0.9770	0.0033
30	0.9780	0.6650	0.7293	0.7946	68	0.9780	0.6650	0.9770	0.0031
31	0.9780	0.6650	0.7359	0.7735	69	0.9780	0.6650	0.9777	0.0010
32	0.9780	0.6650	0.7437	0.7487	70	0.9780	0.6650	0.9777	0.0009
33	0.9780	0.6650	0.7503	0.7276	71	0.9780	0.6650	0.9778	0.0005
34	0.9780	0.6650	0.7568	0.7066	72	0.9780	0.6650	0.9779	0.0004
35	0.9780	0.6650	0.7634	0.6855	73	0.9780	0.6650	0.9779	0.0002
36	0.9780	0.6650	0.7694	0.6664	74	0.9780	0.6650	0.9780	0.0001
37	0.9780	0.6650	0.7766	0.6434	75	0.9780	0.6650	0.9780	0.0001
38	0.9780	0.6650	0.7868	0.6109					

4.3. EXPERIMENTS DESCRIPTION AND MODELING.

4.3.1. SALAMA'S EXPERIMENTS.

In the experiment conducted by Salama (Salama 2006), heavy oil-solvent samples were CT scanned at different times between 0 and 31 hours. From these measurements, concentration evolution with time was estimated.

The oil used had a density of 978 kg/m^3. To set the systems, Hexane, Heptane and Octane were combined with bulk heavy oil. Table 4.3 presents a summary of fluids viscosities at 25˚C.

Table 4.3 Fluids viscosities for Salama's experiment.

	Oil	**Hexane**	**Heptane**	**Octane**
Kinematic viscosity [m^2/s]	1.19E-03	4.46E-07	6.07E-07	5.10E-07

In order to guarantee that only bitumen and solvent were scanned, a region of interest (ROI) inside the vial limits was defined. It encloses the interface between phases that is clearly defined at the beginning of the experiment. The distribution of fluids and ROI location are shown in Figure 4.3.

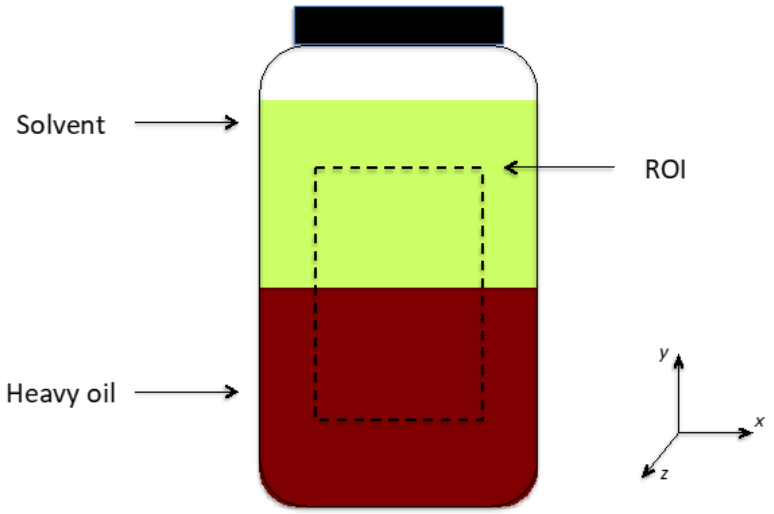

Figure 4.3 Region of interest and initial fluids distribution (Salama 2006)**.**

From Salama's measurements, three solvent concentration profiles at different times are used as a reference for each system analyzed. This is intended to evaluate how the numerical model reproduce the solvent concentration in each system as it evolves with time.

4.3.2. COMPUTATIONAL DOMAIN.

To simulate the experiment, a digital model resembling the Region of Interest (ROI) was constructed. The model is composed of 18,000 cells, thus fulfilling the maximum order of dimensions required for the mesh cells according to the analysis presented in Chapter 3. This was possible by means of local refinement over the interfacial region where diffusion process takes place. Dimensions and initial species concentration are shown in Figure 4.4.

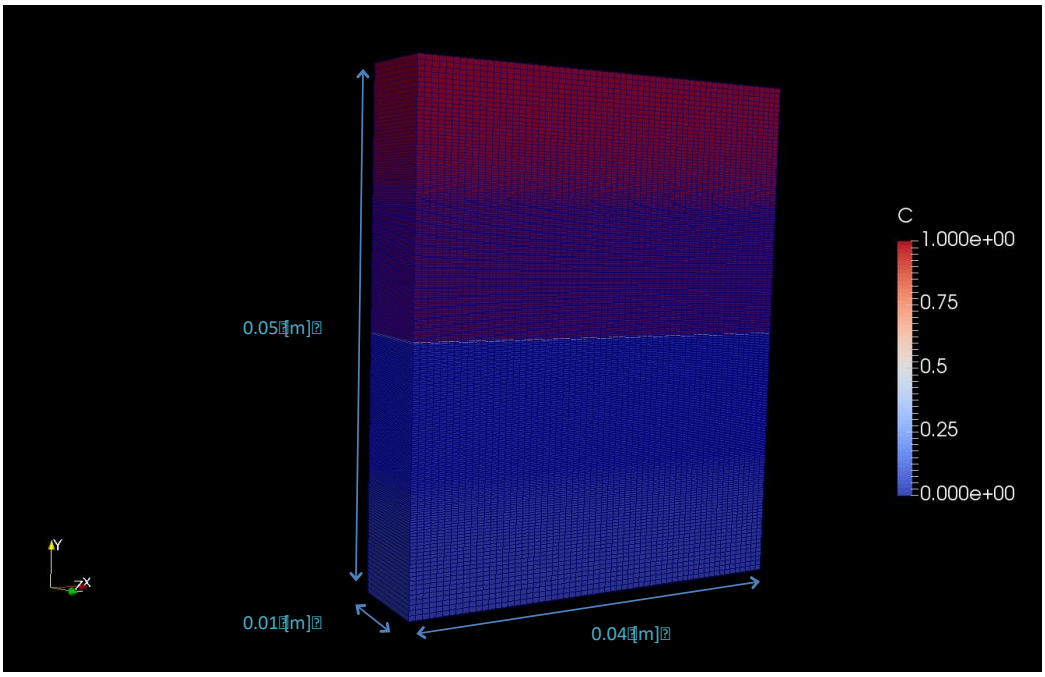

Figure 4.4 Salama's experiment computational domain.

4.3.3. DIEDROS'S EXPERIMENTS.

In the experiments conducted by Diedro (Diedro et al. 2015), two bitumen samples from Peace River (Sand) and Grosmont (Carbonate) formations were combined with solvent and CT scanned. Afterwards, from CT number measurements the concentration evolution with time was estimated. Different from Salama's experiment, the bitumen-solvent systems were run in a horizontal cylindrical holder with bitumen placed below the solvent during different mixing times, Figure 4.5.

From the experiment, the systems including Di-Methyl Ether (DME) as solvent were chosen to be simulated. In table 4.4 the fluids viscosities at 22˚C are summarized.

Table 4.4 Fluids viscosities for Diedro's experiments

	Peace River	Grosmont	DME
Kinematic viscosity [m^2/s]	5.50E-03	1.20E+01	2.24E-05

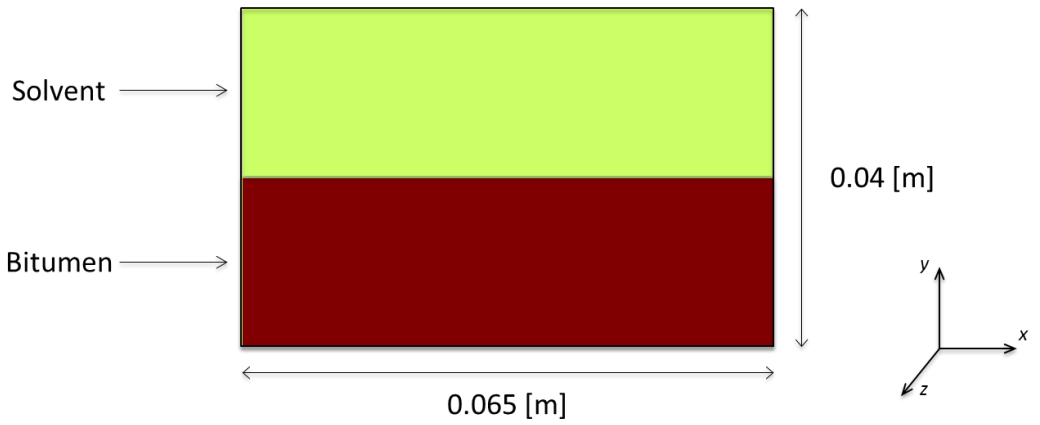

Figure 4.5 Holder dimensions and fluids distribution.

4.3.4. COMPUTATIONAL DOMAIN

Disposed horizontally, the digital model for Diedro's experiments it is also composed by 18,000 cells and refined over the interfacial region. Its dimensions and initial species concentration are shown in Figure 4.6.

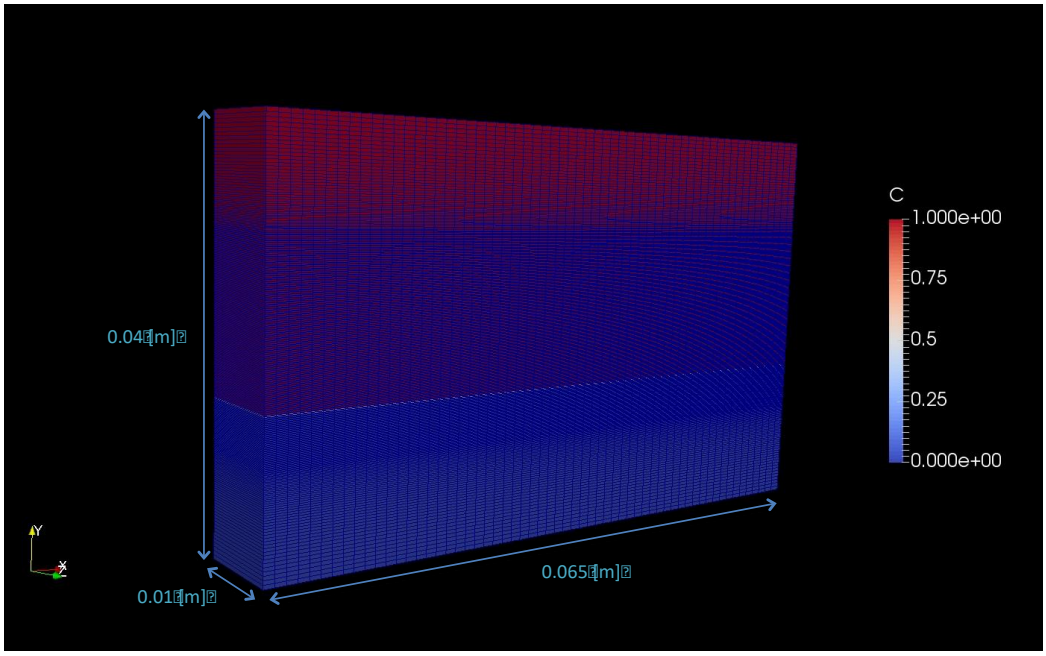

Figure 4.6 Computational domain for Diedro's experiment.

4.4. CONCENTRATION PROFILES EVOLUTION

The measured data are presented as solvent/bitumen concentration profiles showing their evolution against distance at specific times in the experiment. According to measurements of carbon dioxide diffusivity in oil conducted by Nguyen (Nguyen 1997), the diffusion process in binary systems can be divided in three stages.

In the first stage, concentration equilibrium is developed at the interface. The second stage corresponds to the diffusion period, where variation in concentration occurs gradually. Finally, in the third stage, the diffusing fluid reaches the system boundary. Once this happens, the infinite boundary condition, generally assumed to solve the Fick's second law, is not valid anymore.

This can be better explained with aid of Figure 4.7, where data corresponding to the mixing zone length of an octane-oil system are plotted (Salama 2006). In there, it is possible to identify the stages of diffusion process.

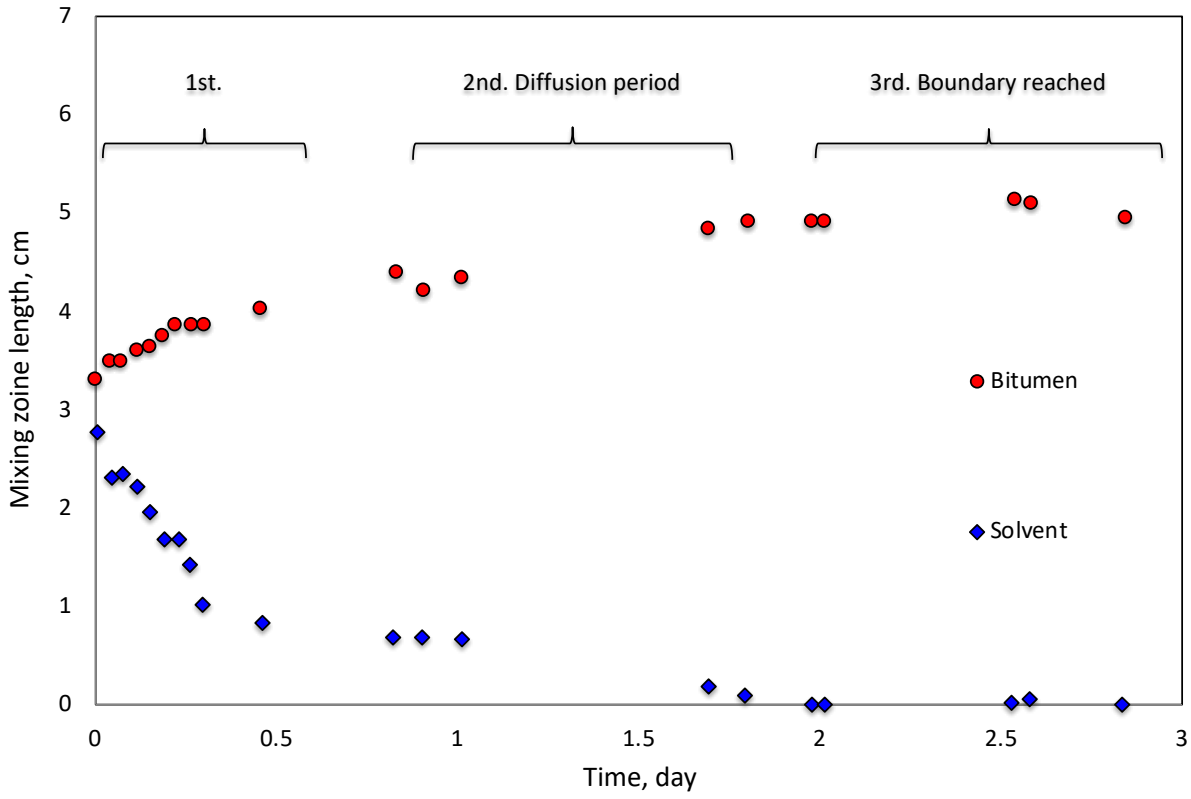

Figure 4.7 Mixing zone length with time (octane-oil), (Salama 2006)**.**

It can be observed that higher length variations occur during the first stage. This can be associated to high diffusivities due to contrast of fluid properties at the interface (Zhang, Fulem, and Shaw 2007). In the diffusion period the mixing zone continues growing but now gradually, until it reaches the system boundaries and no more changes are observed.

This is a key aspect for the CT scan measurements. Since the data obtained was used to determine diffusion coefficients, researchers had to assure that they belong to the diffusion

period for diffusion coefficient computations to be valid. Therefore, in this work, the concentration profiles simulated were measured at times when diffusion period has already started.

4.5. Experiment vs. Modeling

In order to evaluate the performance of simulation models developed, graphical comparisons between concentration data and those simulated with the Concentration Dependent Diffusion Polynomial (CDDP) (Sarafianos 1986) and Vignes Modified (Mendoza et al. 2018) models, are presented for each experiment.

4.5.1. Salama's experiment modeling.

Concentration profiles for the systems Hexane/Heptane/Octane-heavy oil at different times are showed in Figures 4.8 to 4.16.

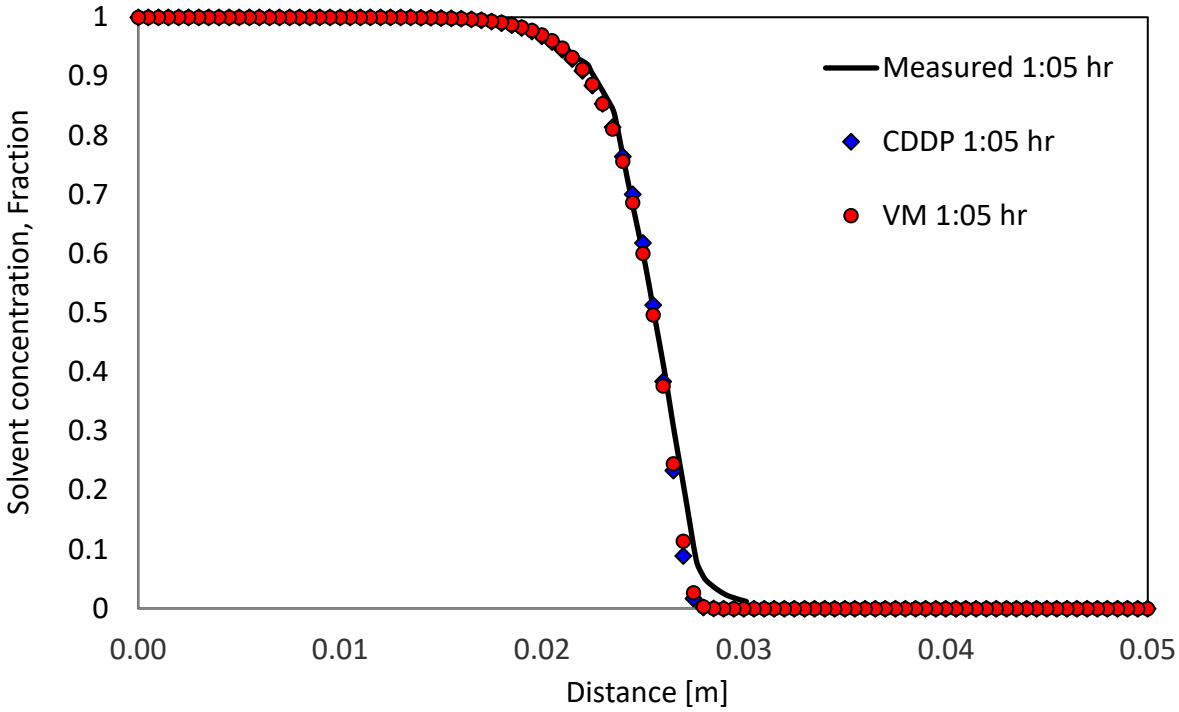

Figure 4.8 Concentration profiles for hexane in heavy oil (1:05 h).

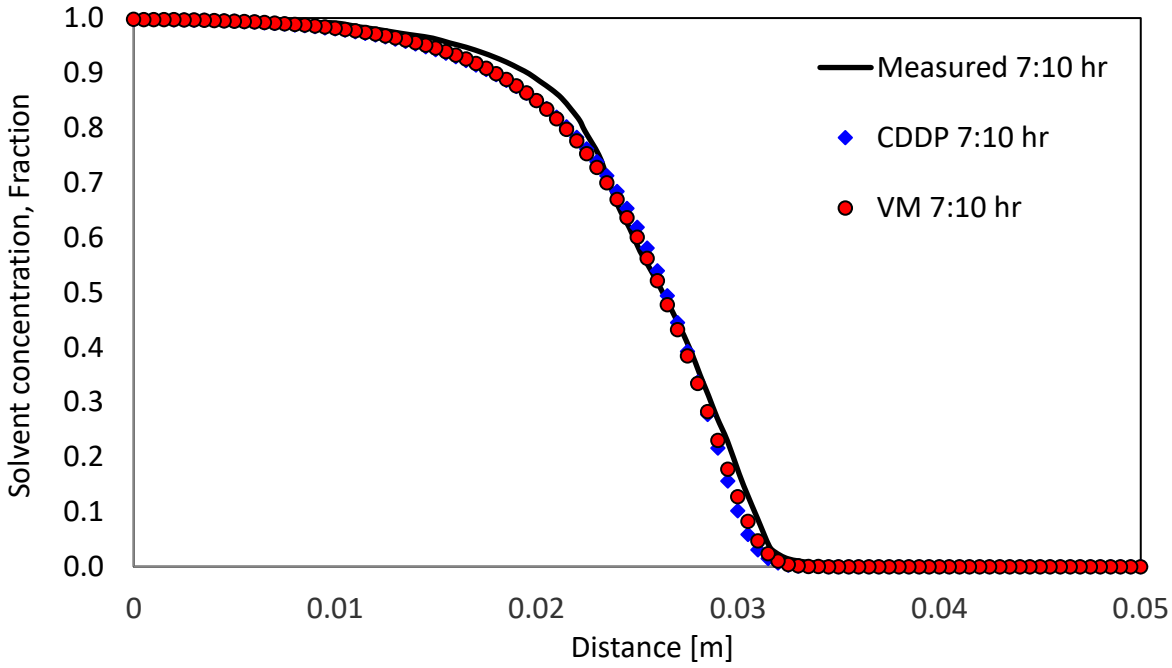

Figure 4.9 Concentration profiles for hexane in heavy oil (7:10 h).

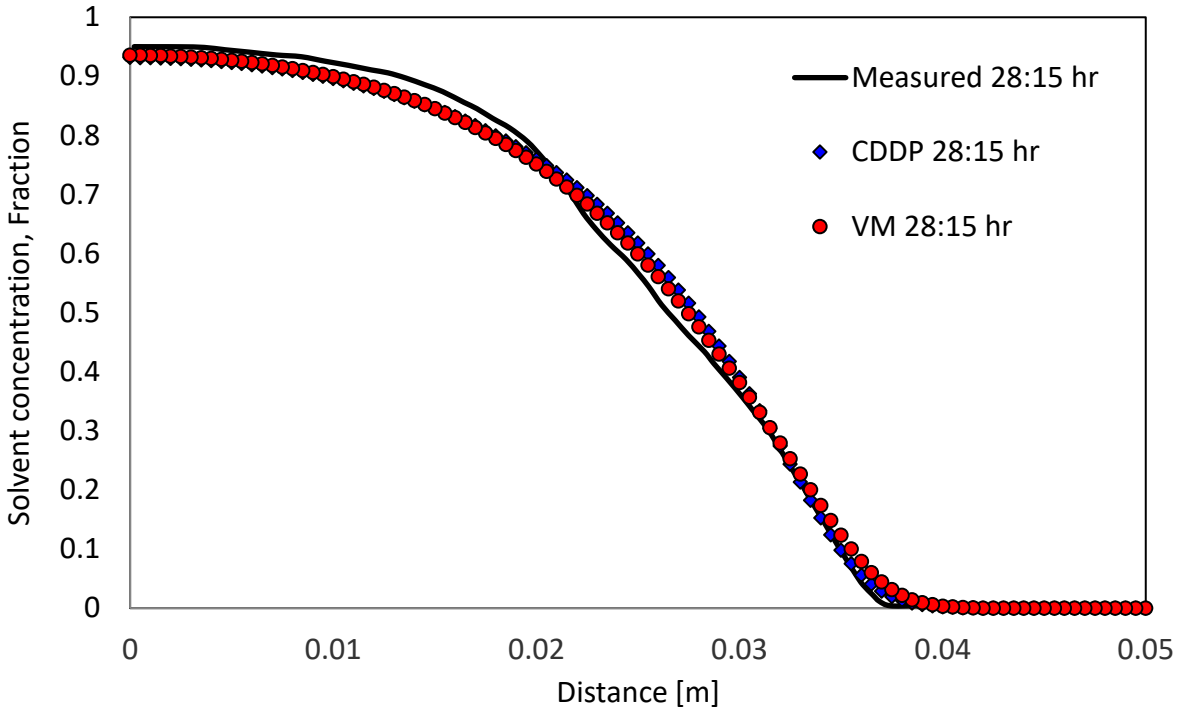

Figure 4.10 Concentration profiles for hexane in heavy oil (28:15 h).

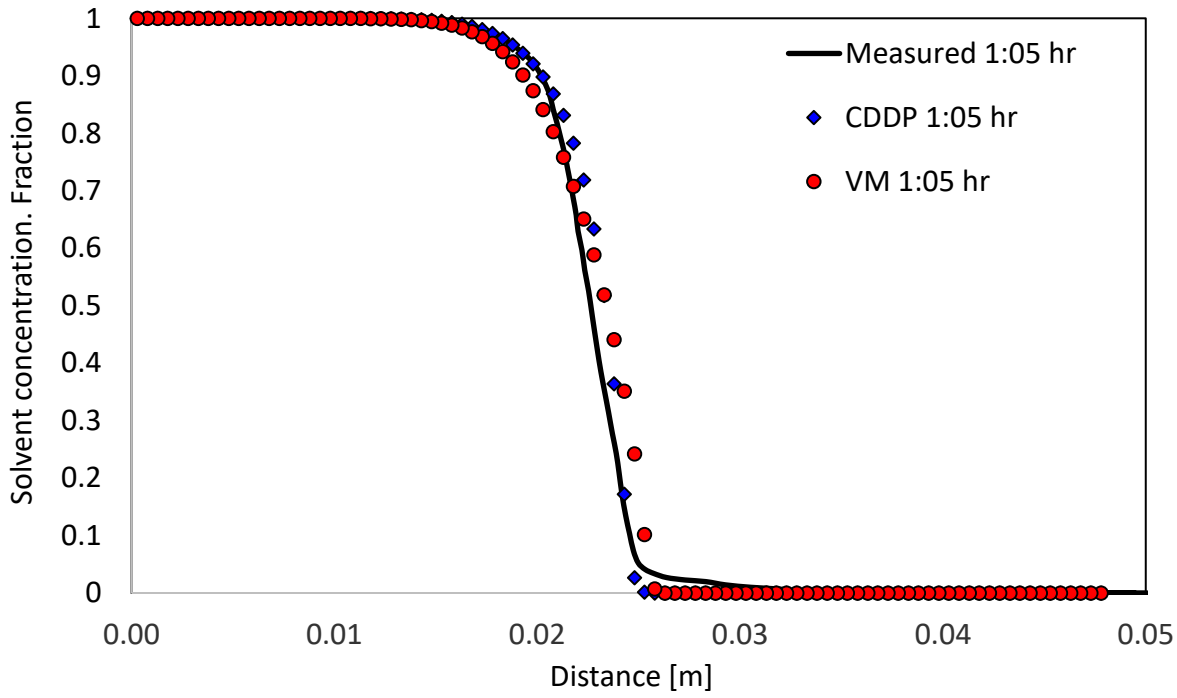

Figure 4.11 Concentration profiles for heptane in heavy oil (1:05 h).

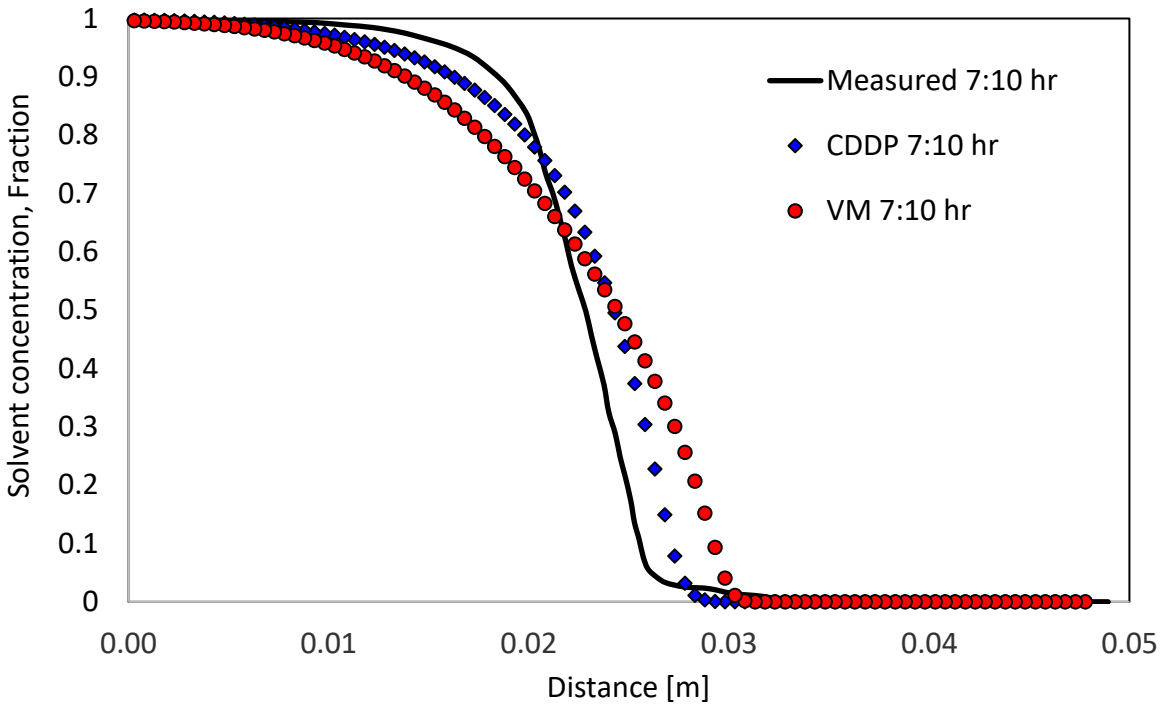

Figure 4.12 Concentration profiles for heptane in heavy oil (7:10 h).

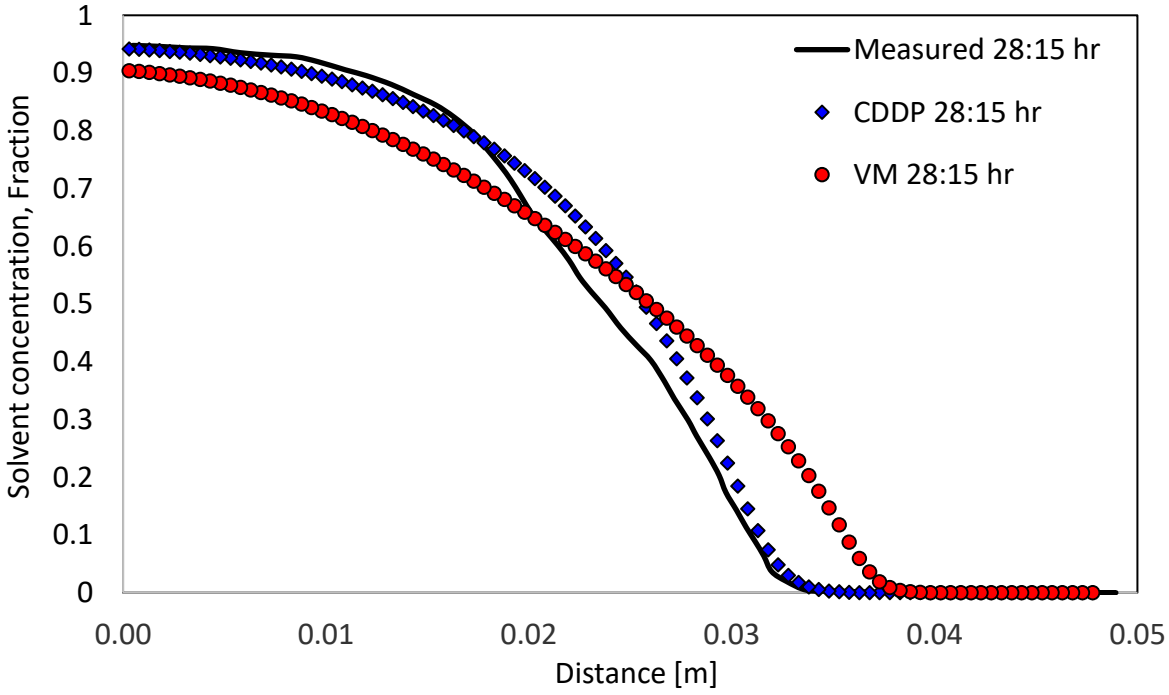

Figure 4.13 Concentration profiles for heptane in heavy oil (28:15 h).

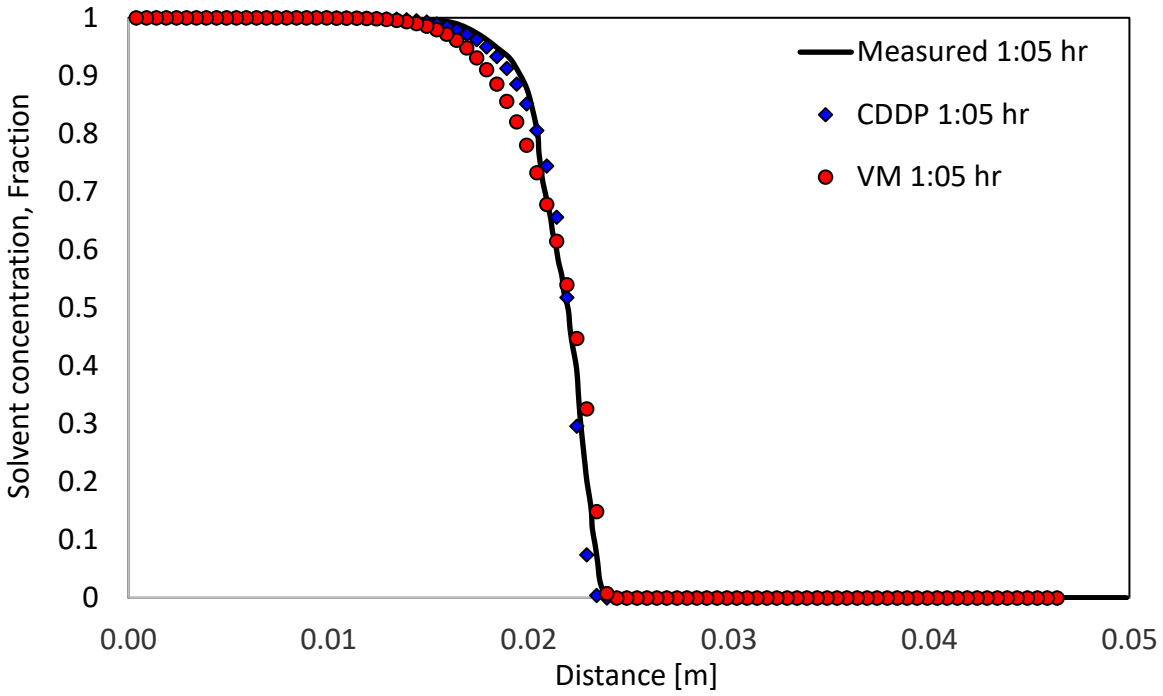

Figure 4.14 Concentration profiles for octane in heavy oil (1:05 h).

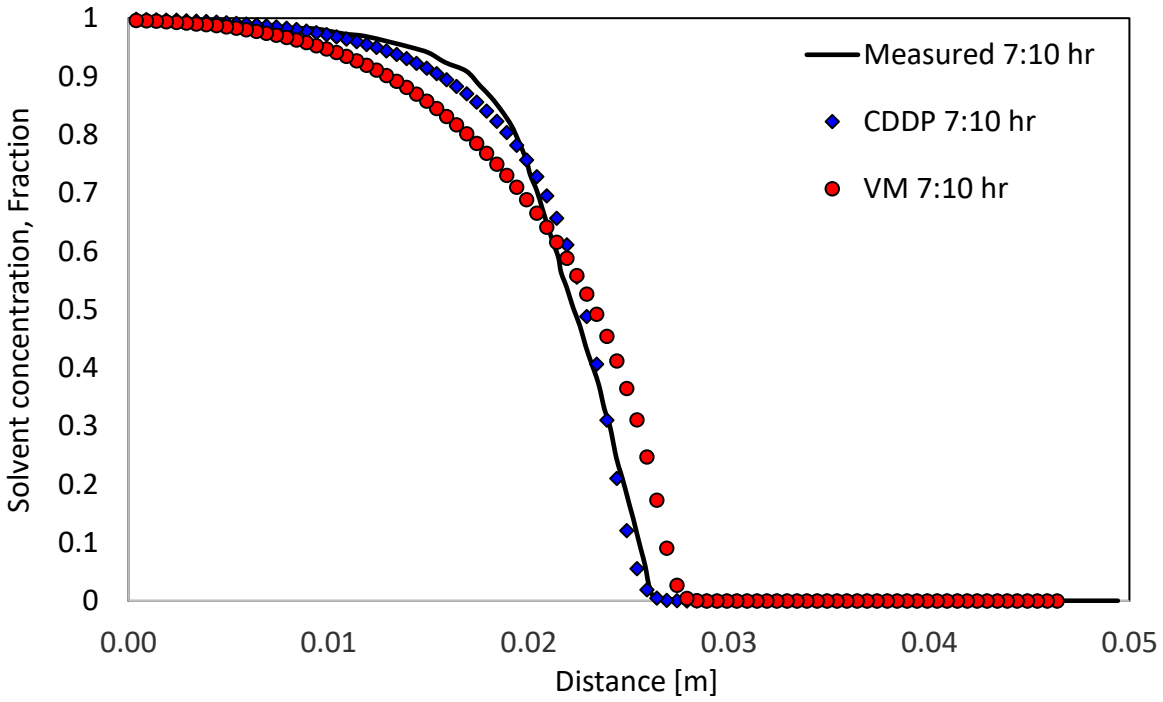

Figure 4.15 Concentration profiles for octane in heavy oil (7:10 h).

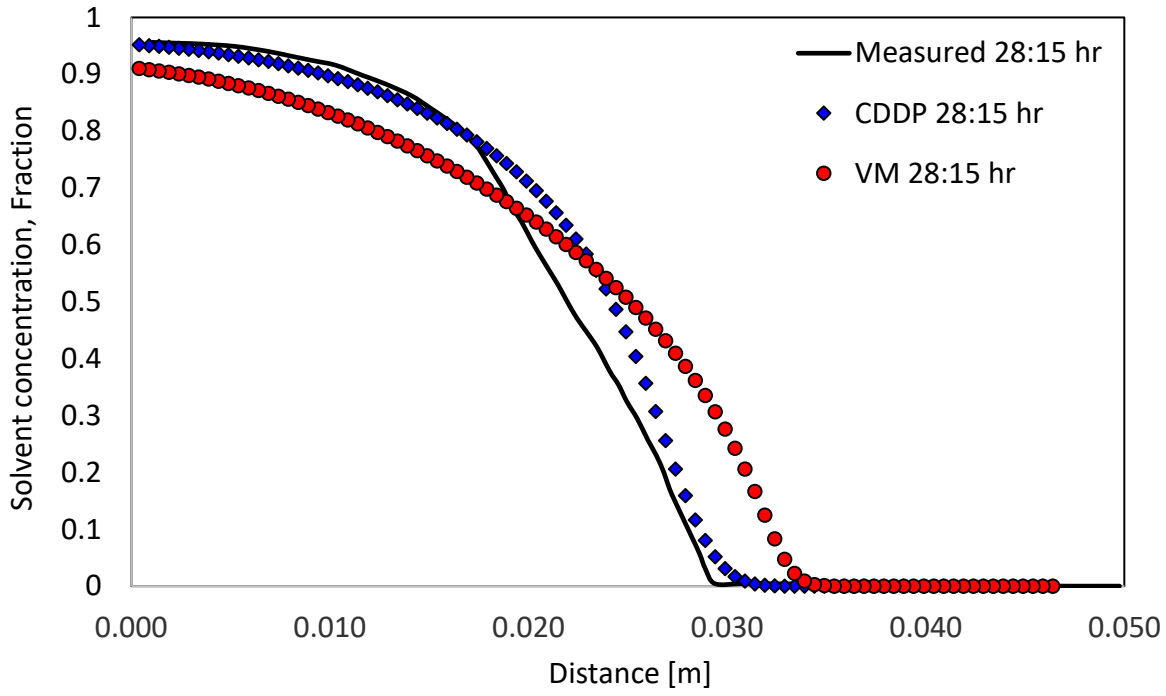

Figure 4.16 Concentration profiles for octane in heavy oil (28:15 h).

In addition to the interfacial diffusion feature validation, this comparison allows to evaluate the solvent concentration dependent characteristic. At glance, the CDDP model gives a closer representation of the concentration dependent mass transfer phenomenon for all the cases.

Figure 4.17 shows the absolute error between measured and simulated data for the solvent-heavy oil systems in Salama's experiments.

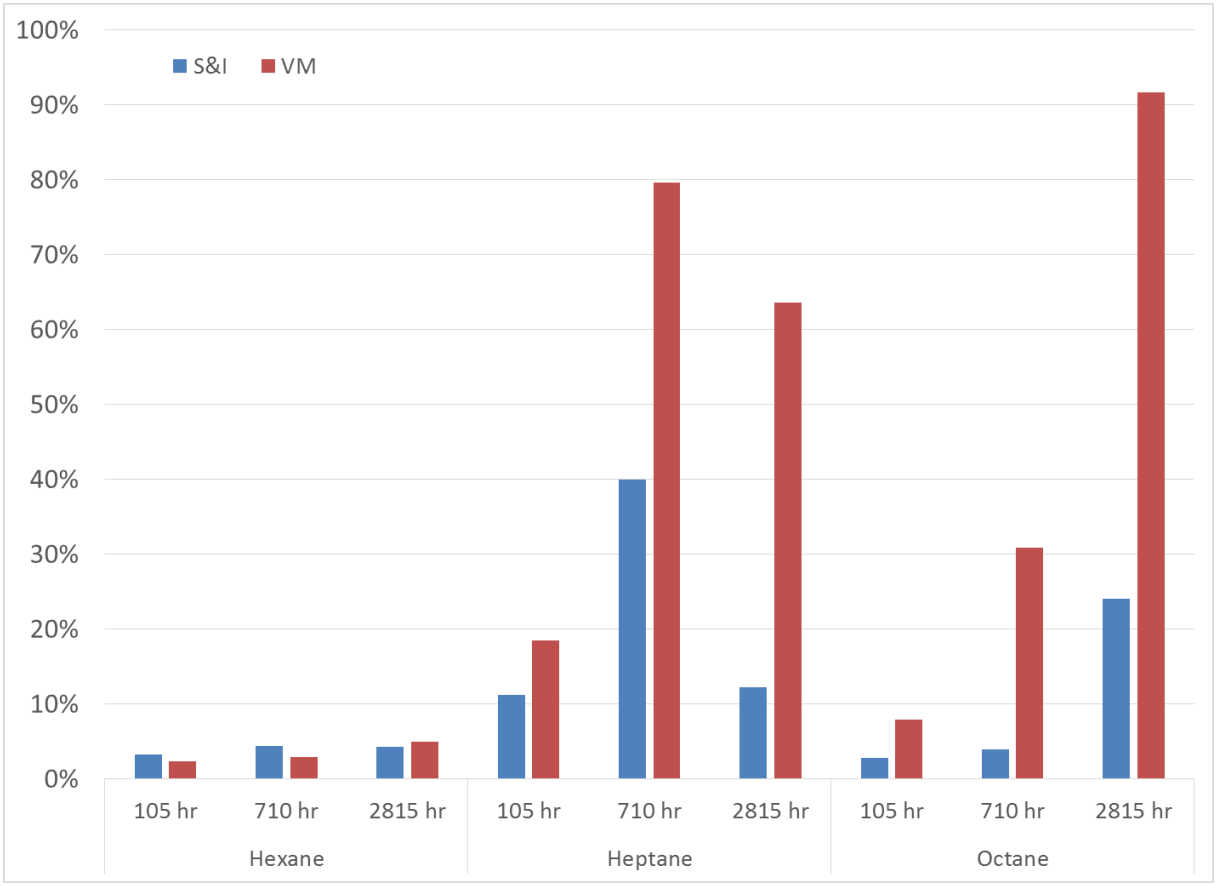

Figure 4.17 Absolute errors between simulated and measured concentration data, Salama's experiment.

Hexane and octane simulations, for instance, show a reasonable deviation that increases with time for the CDDP model. The Vignes Modified model performance, on the other hand, regardless to show a definite error – time correlation for hexane and octane systems, for the second, is at least three orders of magnitude higher when compared to the previous time lapse.

The heptane system simulation not only shows a larger deviation than hexane and octane for all times, but also, this does not correlate with the increasing time for both models.

This behaviour may be attributed to the changes at the interface occurring while solvent is diffusing into the oil.

According to the Salama's interface height evolution analysis, it can be said that the relation observed between error and time for hexane and octane systems is the expected. This can be observed in Figure 4.18, where for times in the range 6 to 30 hours, variation of the mixing zone length is more severe. Starting with a gradual behaviour at early times, passing through intense variation at medium times, and finally tending to get stable at later times.

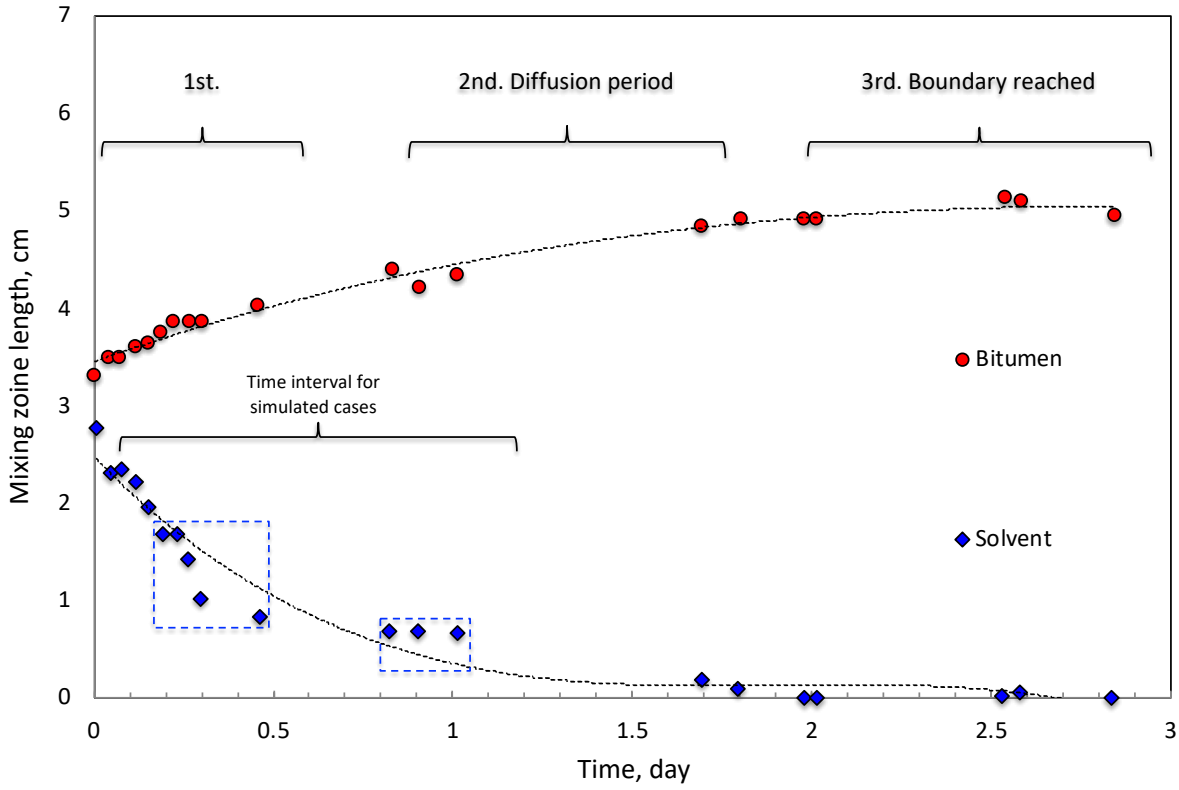

Figure 4.18 Increase of the length of the mixing zone (Salama 2006).

Therefore, the intensification in the activity at the interface for medium and later times, demand from the model a more accurate representation, which is not being reproduced under

the current configuration. This condition becomes critical for the Vignes Modified model, turning it into a misrepresentation of the heptane and octane cases.

This behaviour can be attributed to its dependency on the diffusion coefficients at infinite dilution, “deceleration” and “acceleration” parameters. Which, regardless of being better estimated through Mendoza’s than in the original Vignes approach, remain as an assumption of the deviation from the ideality of the system.

4.5.2. DIEDRO’S EXPERIMENT MODELING

Additionally, Diedro’s experiment was also simulated in order to assess the model capabilities to handle high viscous fluids.

It’s worth mentioning that systems in this experiment pose the fluids with highest viscosity, which effect can be identified in the concentration profiles showed in Figures 4.19 to 4.22. For bitumen concentrations > 0.5, an almost linear trend is described for both Peace River and Grosmont systems, being more noticeable for later times, Figures 4.20 and 4.22.

It can be also noticed that for the high bitumen concentration region (>0.5), the CDDC model shows a good agreement with measured data, except for the Grosmont system at 1 day. However, in lower solvent concentration region considerable, deviation is present for all the cases. This can be attributed to the effect that high solvent concentration has on bitumen, which leads to a free solvent phase, where both models fail to reproduce the concentration profiles evolution.

The Grosmont system simulation for later time, conducted with the Vignes Modified model, is clearly the most deviated, Figure 4.21. This exercise stands for the less ideal system, which complicates the model parameters selection when this model is applied.

The results obtained in the simulations of Diedro's experiment, showed a similar behaviour to those for the experiment of Salama, where a better match between measured and simulated concentration profiles was obtained with the CDDP model.

These results let to consider the CDDP model as a valid representation of the components diffusion through an interface in hexane and octane systems when the solvent concentration effect is considered. Since it demonstrates to be able to handle low diffusivities, common in solvent / heavy oil – bitumen systems, and the high contrast between fluid properties at the interface. Nevertheless, the deviations at the middle of concentration range are present, these are due to the diffusion coefficient estimation method´s lack of accuracy, which are only present in this region of the curve.

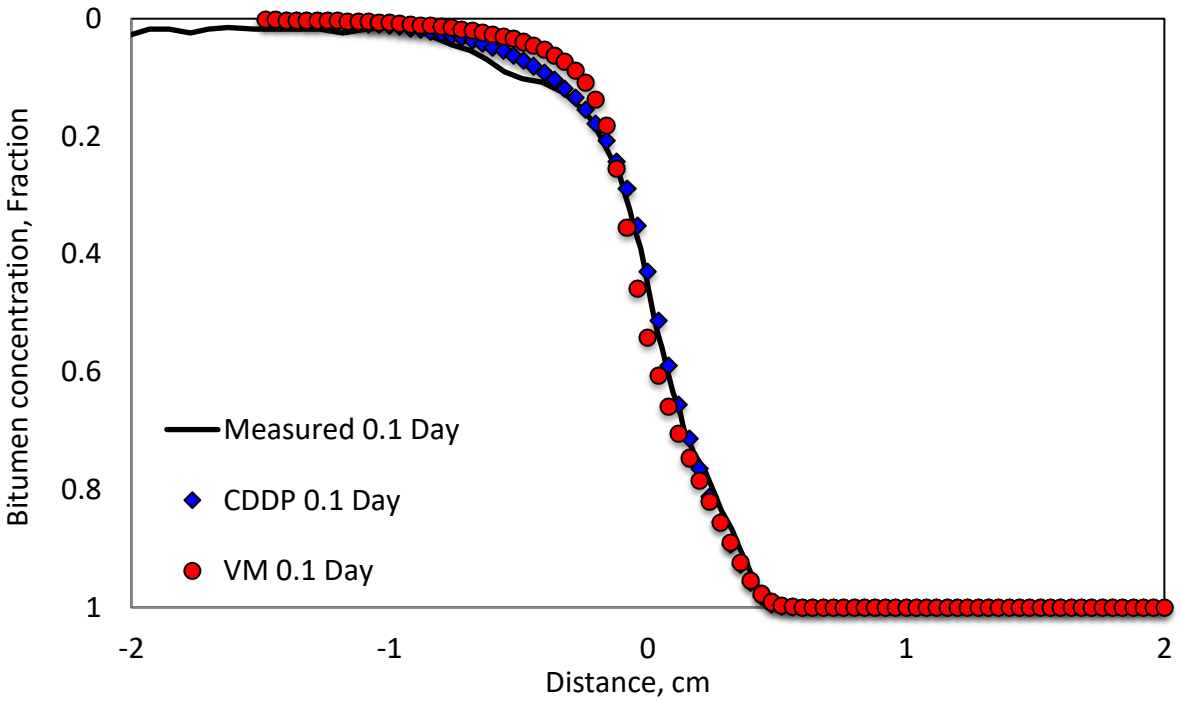

Figure 4.19 Concentration profiles for Peace River bitumen and DME (0.1 day).

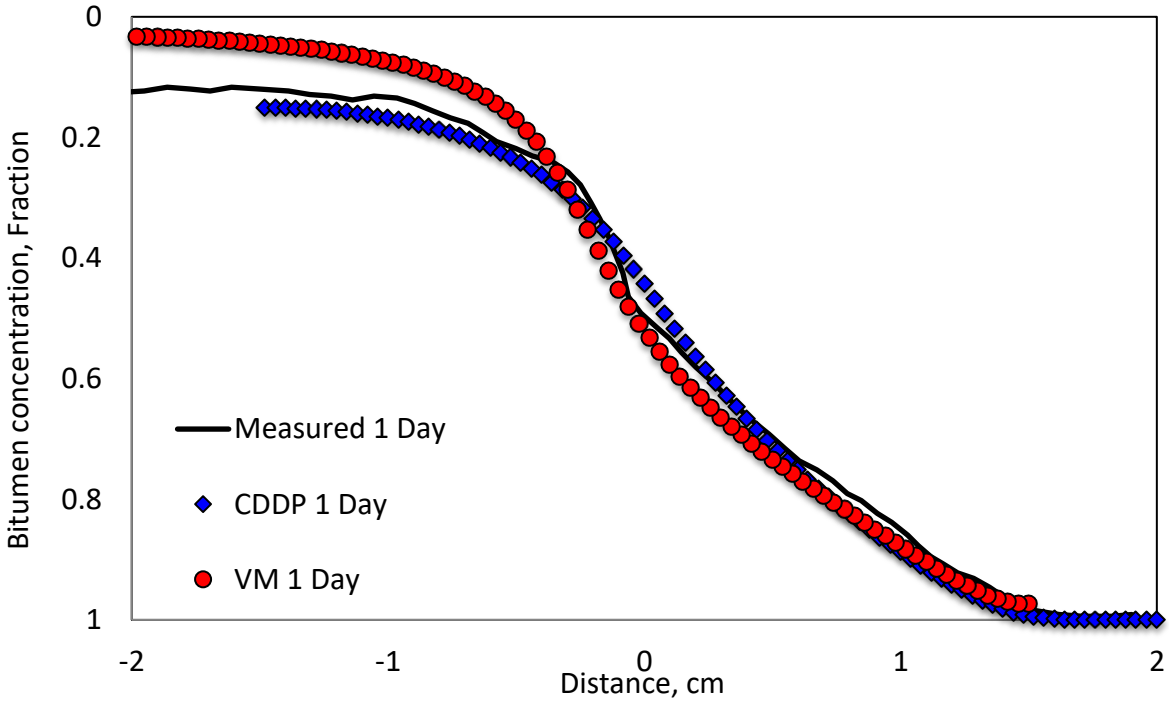

Figure 4.20 Concentration profiles for Peace River bitumen and DME (1 day).

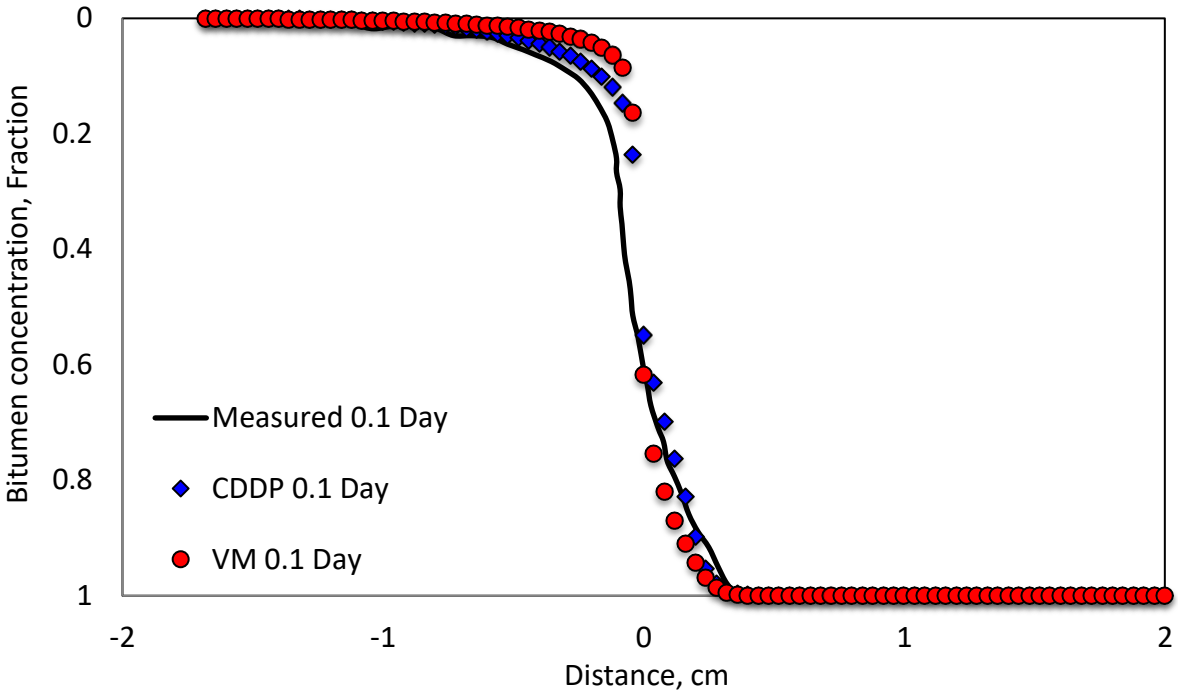

Figure 4.21 Concentration profiles for Grosmont bitumen and DME (0.1 day).

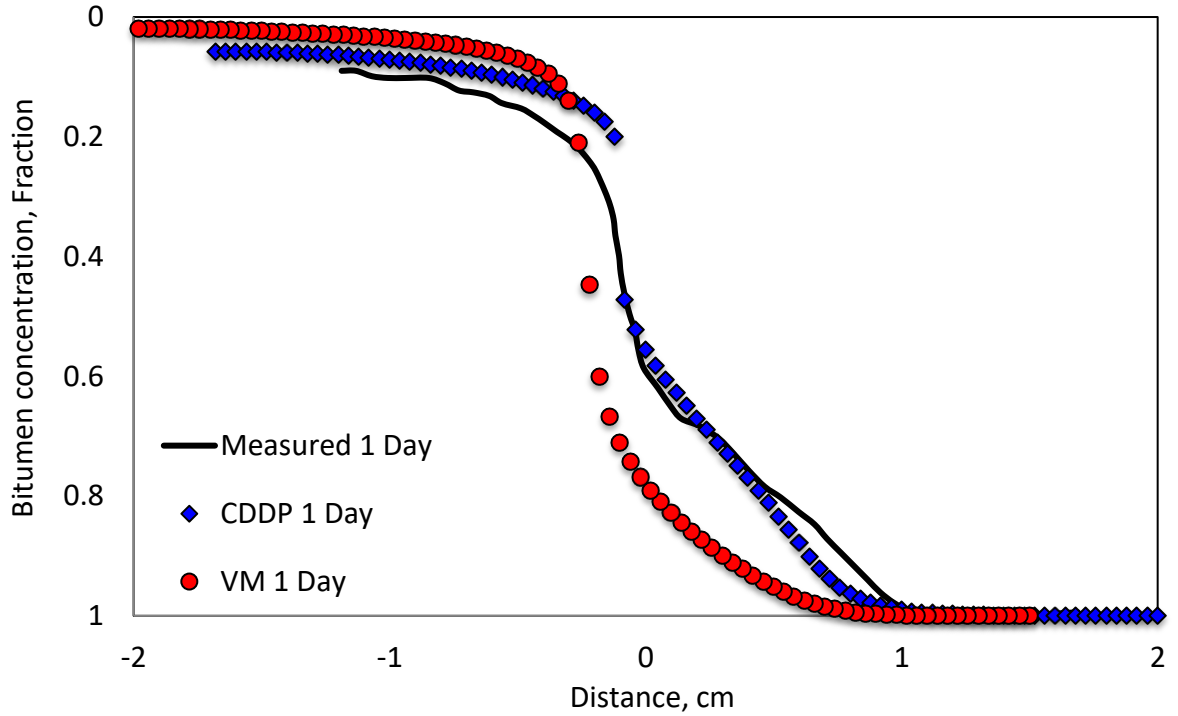

Figure 4.22 Concentration profiles for Grosmont bitumen and DME (1 day).

The average absolute error for Diedro's experiment simulations are presented in Figure 4.23.

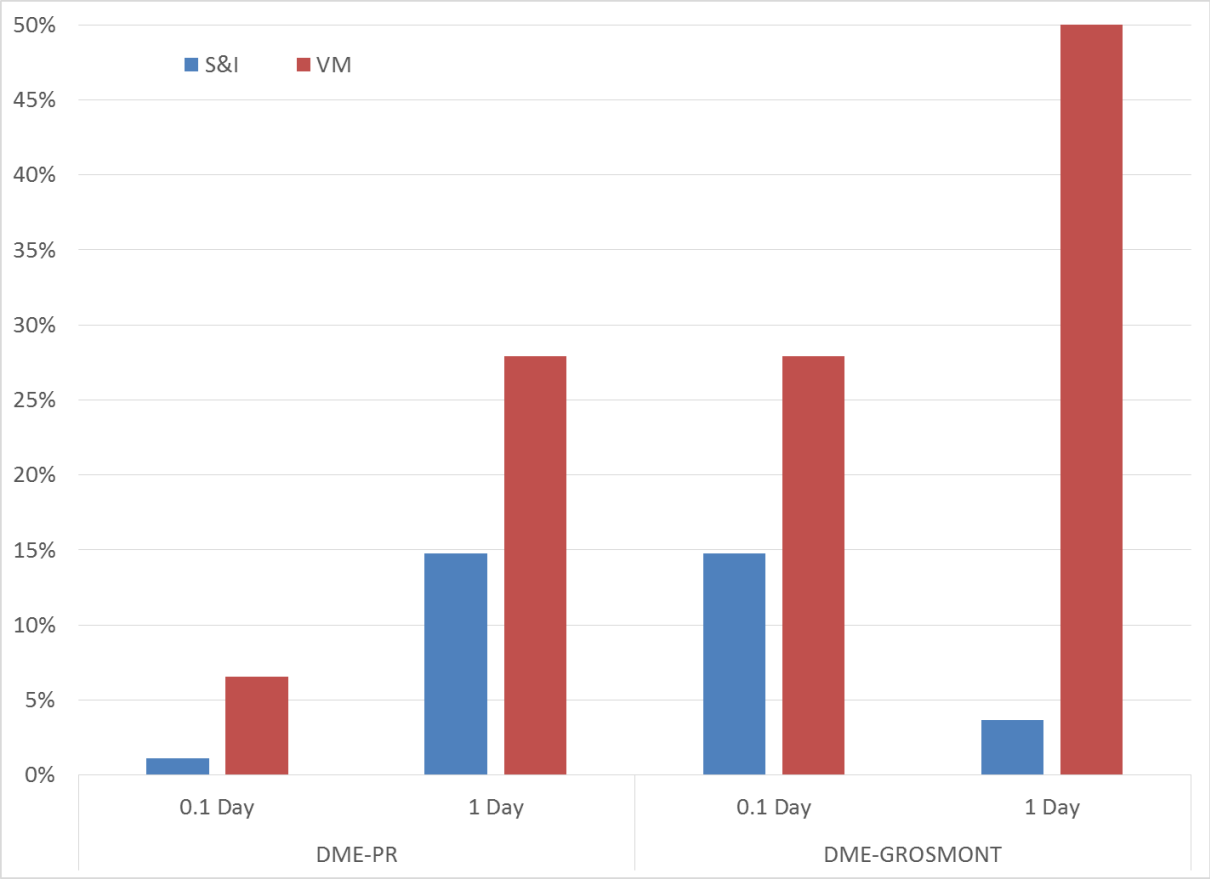

Figure 4.23 Absolute errors between simulated and measured concentration data.

CHAPTER 5. CONCLUSIONS AND FUTURE WORK

5.1. FINAL CONCLUSIONS

In this study, the interfacial diffusion of a miscible solvent between two phases has been analysed. From the results obtained the following conclusions can be drawn:

1. A numerical model in the open source code OpenFOAM able to simulate low diffusion coefficients dependent on solvent concentration, under the VOF method, has been developed.

2. The assumption of static conditions remains valid given the experimental setup used for the X-ray measurements, and due to diffusion occurs between liquids.

3. Advection free diffusivity is verified at early, intermediate and later times for CDDP and VM models for hexane system.

4. The simulation results of the CDDP model show a good agreement for the three systems, losing accuracy for later times.

5. The CDDP model performance is influenced by the adjustment of the polynomial relations describing variable diffusion coefficients.

6. The performance of the VM model strongly depends on the calculation of δ and β adjustment parameters.

5.2. RECOMMENDATIONS

This study was conducted intending to develop a volume of fluid based numerical model that helps to understand the diffusion process at the interface between fluids involved in solvent assisted process. The model presented can capture the concentration effect on the diffusion coefficient, which is the main objective of this thesis. Nevertheless, in order to increase its application spectrum, additional work is needed. Below, recommendations for future research are listed:

This research needs further study to extend its application to solvents in gaseous phase. Likewise, additional physics related to mass transfer by diffusion in hydrocarbon solvent – heavy oil / bitumen system need to be investigated. For instance, phases volume changes and viscosity variations due mass transfer.

Additional models describing the diffusion coefficient as a function of concentration need to be assessed in order to improve the description of fluids concentration evolution even for concentration ranges causing severe physical changes at the interface.

Furthermore, conduct additional testing on the oil produced from the Grosmont reservoir, given its properties.

It is also recommended to run simulations in porous media patterns, aimed to determine the effect that topology media has on a concentration dependent diffusion process.

REFERENCES

Ahadi, Arash and Farshid Torabi. 2018. “Insight into Heavy Oil Recovery of Cyclic Solvent Injection (CSI) Utilizing C3H8/CH4 and C3H8/CH4/CO2.” *Petroleum*.

Allen, Joseph C., Charles D. Woodward, Alfred Brown, and Ching H. Wu. 1976. “Multiple Solvent Heavy Oil Recovery Method.”

Ardali, M., M. A. Barrufet, and D. D. Mamora. 2012. “A Critical Review of Hybrid Steam/Solvent Processes to Recover Heavy Oil. Paper SPE 159257 Presented at SPE Annual Technical Conference and Exhibition, San Antonio, Texas, 8–10 October.”

Badalassi, V. E., H. D. Ceniceros, and Sanjoy Banerjee. 2003. “Computation of Multiphase Systems with Phase Field Models.” *Journal of Computational Physics* 190(2):371–97.

Bardon, C. P., D. Karaoguz, and M. Tholance. 1986. “Well Stimulation by CO2 in the Heavy Oil Field of Camurlu in Turkey.” in *SPE Enhanced Oil Recovery Symposium*. Society of Petroleum Engineers.

Bayestehparvin, Bita, S. M. Farouq Ali, and Jalal Abedi. 2018. “Solvent-Based and Solvent-Assisted Recovery Processes: State of the Art.” *SPE Reservoir Evaluation & Engineering*.

Boltzmann, Ludwig. 1894. “Zur Integration Der Diffusionsgleichung Bei Variabeln Diffusionscoefficienten.” *Annalen Der Physik* 289(13):959–64.

Bothe, D. and H. J. Warnecke. 2005. “VOF-Simulation of Rising Air Bubbles with Mass Transfer to the Ambient Liquid.” Pp. 61–72 in *10th Workshop on Transport Phenomena in Two-phase Flow*.

Brackbill, J. U., Douglas B. Kothe, and Charles Zemach. 1992. “A Continuum Method for Modeling Surface Tension.” *Journal of Computational Physics* 100(2):335–54.

Butler, R. M. and Igor J. Mokrys. 1989. “Solvent Analog Model of Steam-Assisted Gravity Drainage.” 5:17–32.

Butler, Roger M. and IGOR J. Mokrys. 1991. “A New Process (VAPEX) for Recovering Heavy Oils Using Hot Water and Hydrocarbon Vapour.” *Journal of Canadian Petroleum Technology* 30(01).

Chang, Jeannine and John Ivory. 2013. “Field-Scale Simulation of Cyclic Solvent Injection (CSI).” *Journal of Canadian Petroleum Technology* 52(04):251–65.

Cinar, Yildiray and Amir Riaz. 2014. “Carbon Dioxide Sequestration in Saline Formations: Part 2—Review of Multiphase Flow Modeling.” *Journal of Petroleum Science and Engineering* 124:381–98.

Crank, John. 1979. *The Mathematics of Diffusion*. Oxford university press.

Das, Swapan K. 1998. “Vapex: An Efficient Process for the Recovery of Heavy Oil and Bitumen.” *SPE Journal* 3(03):232–37.

Das, Swapan K. and Roger M. Butler. 1996. “Diffusion Coefficients of Propane and Butane in Peace River Bitumen.” *The Canadian Journal of Chemical Engineering* 74(6):985–92.

Deising, Daniel, Holger Marschall, and Dieter Bothe. 2016. “A Unified Single-Field Model Framework for Volume-Of-Fluid Simulations of Interfacial Species Transfer Applied to Bubbly Flows.” *Chemical Engineering Science* 139:173–95.

Deshpande, Suraj S., Lakshman Anumolu, and Mario F. Trujillo. 2012. “Evaluating the Performance of the Two-Phase Flow Solver InterFoam.” *Computational Science & Discovery* 5(1):14016.

Diedro, Franck, Jonathan Bryan, Sergey Kryuchkov, and Apostolos Kantzas. 2015. “Evaluation of Diffusion of Light Hydrocarbon Solvents in Bitumen.” Calgary: Society of Petroleum Engineers.

Du, Zhongwei, Xiaolong Peng, and Fanhua Zeng. 2018. “Comparison Analyses between the Linear and Non-Linear Pressure-Decline Methods in Cyclic Solvent Injection (CSI) Process for Heavy Oil Recovery.” *Fuel* 224:442–50.

Emad, Vahid. 2014. “Evaluating the Performance of Various Convection Schemes on Free Surface Flows by Using Interfoam Solver.” Doctoral dissertation, Eastern Mediterranean University, Fagamusta, Cyprus.

Fadaei, Hossein, John M. Shaw, and David Sinton. 2013. “Bitumen–toluene Mutual Diffusion Coefficients Using Microfluidics.” *Energy & Fuels* 27(4):2042–48.

Ghanavati, Mohsen, Hassan Hassanzadeh, and Jalal Abedi. 2014. “Critical Review of Mutual Diffusion Coefficient Measurements for Liquid Solvent+ Bitumen/Heavy Oil Mixtures.” *The Canadian Journal of Chemical Engineering* 92(8):1455–66.

Graveleau, Marguerite. 2016. “Pore-Scale Simulation of Mass Transfer Across Immiscible Interfaces.” Master's thesis, Stanford University, Palo Alto, United States.

Groß, Sven and Arnold Reusken. 2013. “Numerical Simulation of Continuum Models for Fluid-Fluid Interface Dynamics.” *The European Physical Journal Special Topics* 222(1):211–39.

Guerrero-Aconcha, Uriel Enrique. 2009. “The Diffusion Coefficient of Liquid and Gaseous Solvents in Heavy Oil and Bitumen.” Master's thesis, University of Calgary, Calgary, Canada.

Guo, Kun, Hailong Li, and Zhixin Yu. 2016. “In-Situ Heavy and Extra-Heavy Oil Recovery: A Review.” *Fuel* 185:886–902.

Haddad, Amin Sharifi, S. Hossein Hejazi, and Ian D. Gates. 2017. “Modeling Solvent Enhanced Gravity Drainage from a Single Matrix Block in Fractured Oil Reservoirs.”

Journal of Petroleum Science and Engineering 152:555–63.

Haroun, Yacine. 2008. "Etude Du Transfert de Masse Réactif Gaz-Liquide Le Long de Plans Corrugués Par Simulation Numérique Avec Suivi d'interface." Doctoral dissertation, Université de Toulouse, Toulouse, France.

Hayduk, W. and S. C. Cheng. 1971. "Review of Relation between Diffusivity and Solvent Viscosity in Dilute Liquid Solutions." *Chemical Engineering Science* 26(5):635–46.

Hirt, Cyril W. and Billy D. Nichols. 1981. "Volume of Fluid (VOF) Method for the Dynamics of Free Boundaries." *Journal of Computational Physics* 39(1):201–25.

Jamaloei, Benyamin Yadali, Mingzhe Dong, Ping Yang, Daoyong Yang, and Nader Mahinpey. 2013. "Impact of Solvent Type and Injection Sequence on Enhanced Cyclic Solvent Process (ECSP) for Thin Heavy Oil Reservoirs." *Journal of Petroleum Science and Engineering* 110:169–83.

Kantzas, A. 1990. "Investigation of Physical Properties of Porous Rocks and Fluid Flow Phenomena in Porous Media Using Computer Assisted Tomography." *In Situ;(USA)* 14(1).

Kantzas, Apostolos. 1994. "Computation of Holdups in Fluidized and Trickle Beds by Computer-assisted Tomography." *AIChE Journal* 40(7):1254–61.

Keshmiri, Kiarash, Mohammad Pourmohammadbagher, Haibo Huang, and Neda Nazemifard. 2019. "Microfluidics to Determine the Diffusive Mass Transfer of a Low Viscosity Solvent into a High Viscosity Hydrocarbon." *Fuel* 235:1327–36.

Leyva-Gomez, Hector and Tayfun Babadagli. 2018. "Efficiency of Heavy-Oil/Bitumen Recovery from Fractured Carbonates by Hot-Solvent Injection." *Journal of Petroleum Science and Engineering* 165:752–64.

Lin, Lixing, Hongze Ma, Fanhua Zeng, and Yongan Gu. 2014. "A Critical Review of the Solvent-Based Heavy Oil Recovery Methods." in *SPE Heavy Oil Conference-Canada*. Society of Petroleum Engineers.

Luo, Kun, Changxiao Shao, Yue Yang, and Jianren Fan. 2015. "A Mass Conserving Level Set Method for Detailed Numerical Simulation of Liquid Atomization." *Journal of Computational Physics* 298:495–519.

Luo, Peng, Chaodong Yang, and Yongan Gu. 2007. "Enhanced Solvent Dissolution into In-Situ Upgraded Heavy Oil under Different Pressures." *Fluid Phase Equilibria* 252(1–2):143–51.

Marciales, Andrea and Tayfun Babadagli. 2016. "Solvent-Selection Criteria Based on Diffusion Rate and Mixing Quality for Steam/Solvent Applications in Heavy-Oil and Bitumen Recovery." *SPE Reservoir Evaluation & Engineering* 19(04):620–32.

Márquez-Damián, Santiago. n.d. *Description and Utilization of InterFoam Multiphase Solver*.

Matano, Chujiro. 1933. “On the Relation between the Diffusion-Coefficients and Concentrations of Solid Metals.” *Japanese Journal of Physics* 8:109–13.

Mendoza, Ana, Petro Babak, and Apostolos Kantzas. 2018. “Estimation and Prediction of Diffusion Coefficients in Liquid Solvent Bitumen Systems.” *Energy & Fuels* 32(11):11143–52.

Nasr, T. N., G. Beaulieu, H. Golbeck, and G. Heck. 2002. “Novel Expanding Solvent-SAGD Process ‘ES-SAGD.’” in *Canadian International Petroleum Conference*. Petroleum Society of Canada.

Nguyen, Tai A. 1997. “Scaled Model Studies of the Immiscible Carbon Dioxide WAG Flooding Process under Various Conditions.” University of Alberta.

Oballa, Viera and R. M. Butler. 1989. “An Experimental Study of Diffusion in the Bitumen-Toluene System.” *Journal of Canadian Petroleum Technology* 28(02).

Osher, Stanley and James A. Sethian. 1988. “Fronts Propagating with Curvature-Dependent Speed: Algorithms Based on Hamilton-Jacobi Formulations.” *Journal of Computational Physics* 79(1):12–49.

Peaceman, Donald W. 2000. *Fundamentals of Numerical Reservoir Simulation*. Vol. 6. Elsevier.

Pourabdollah, Kobra and Bahram Mokhtari. 2013. “The VAPEX Process, from Beginning up to Date.” *Fuel* 107:1–33.

Qi, J. and M. Polikar. 2005. “Optimal Solvent and Well Geometry for Production of Heavy Oil by Cyclic Solvent Injection.” in *Canadian International Petroleum Conference*. Petroleum Society of Canada.

Sabeti, Morteza, Mohammad R. Ehsani, Mohammad Nikookar, and Amir H. Mohammadi. 2015. “Estimation of Effect of Diffusion and Dispersion Parameters on VAPEX Process.” *Journal of Petroleum Science and Engineering* 132:53–64.

Salama, Dalia. 2006. “Monitoring of Hydrocarbon Solvents: Heavy Oil Interactions Using Computed Assisted Tomography.” Master's thesis, University of Calgary, Calgary, Canada.

Santiago, Carla Jordana Sena. 2015. “Two-Phase Flow at the Pore-Scale Using the Volume of Fluid Method.” Master's thesis, University of Calgary, Calgary, Canada.

Sarafianos, N. 1986. “An Analytical Method of Calculating Variable Diffusion Coefficients.” *Journal of Materials Science* 21(7):2283–88.

Sheikha, Hussain, Mehran Pooladi-Darvish, and Anil K. Mehrotra. 2005. “Development of Graphical Methods for Estimating the Diffusivity Coefficient of Gases in Bitumen from Pressure-Decay Data.” *Energy & Fuels* 19(5):2041–49.

Versteeg, H. K. and W. Malalasekera. 2007. *An Introduction to Computional Fluid*

Dynamics: The Finite Volume Method. Pearson Education.

Vignes, Alain. 1966. “Diffusion in Binary Solutions. Variation of Diffusion Coefficient with Composition.” *Industrial & Engineering Chemistry Fundamentals* 5(2):189–99.

Wang, Yanyong, Shaoran Ren, Liang Zhang, and Changhao Hu. 2018. “Energy Efficiency and Greenhouse Gas Emissions of Current Steam Injection Process and Promising Steam Based Techniques for Heavy Oil Reservoirs.” *Journal of Petroleum Science and Engineering* 166:842–49.

Wen, Y. W. and A. Kantzas. 2005. “Monitoring Bitumen− Solvent Interactions with Low-Field Nuclear Magnetic Resonance and X-Ray Computer-Assisted Tomography.” *Energy & Fuels* 19(4):1319–26.

Wörner, Martin. 2012. “Numerical Modeling of Multiphase Flows in Microfluidics and Micro Process Engineering : A Review of Methods and Applications.” *Microfluid Nanofluid* 12:841–86.

Zhang, Xiaohui, Michal Fulem, and John M. Shaw. 2007. “Liquid-Phase Mutual Diffusion Coefficients for Athabasca Bitumen+ Pentane Mixtures.” *Journal of Chemical & Engineering Data* 52(3):691–94.

Zhao, Litong. 2004. “Steam Alternating Solvent Process.” in *SPE International Thermal Operations and Heavy Oil Symposium and Western Regional Meeting*. Society of Petroleum Engineers.

Zhou, Xiang, Qingwang Yuan, Xiaolong Peng, Fanhua Zeng, and Liehui Zhang. 2018. “A Critical Review of the CO 2 Huff ‘n’Puff Process for Enhanced Heavy Oil Recovery.” *Fuel* 215:813–24.